Journal of Nanobiotechnology

RESEARCH

Open Access

Extracellular vesicle-mediated gene therapy targets BRAF^{V600E}-mutant colorectal cancer by inhibiting the MEK1/2-ERK1/2 pathway

Di Wang[1,2,3,4†], Liwei Wang[1,2,3,4†], Wei Zhang[5†], Kaicheng Xu[1,2,3,4], Liang Chen[1,2,3,4], Ziye Guo[1,2,3,4], Kaile Wu[1,2,3,4], Donghua Huang[1,2,3,4], Yubin Zhao[1,2,3,4], Minjun Yao[1,2,3,4], Liming Zheng[1,2,3,4], Chenyi Ye[1,2,3,4], Jisheng Ran[1,2,3,4], Wei Zhou[5*], Xin Liu[6*] and Jianbin Xu[1,2,3,4*]

Abstract

Background Patients with colorectal cancer (CRC) harboring BRAF mutation have a poor prognosis. The median survival time for patients with advanced BRAF^{V600E}-mutant CRC is only approximately one year. Owing to the insensitivity to standard chemotherapy, there are still no effective and highly specific treatment strategies available in clinical practice for CRC patients with BRAF mutation. Therefore, targeting the BRAF^{V600E} mutation site, researching and exploring novel targeted therapies are essential to improve the survival rate of patients with this CRC subtype.

Aim This study aims to develop a precise therapeutic system for BRAF^{V600E} CRC, based on the carrier properties of extracellular vesicles (EVs) and gene therapy targeting BRAF^{V600E}.

Method We first obtained engineered cells capable of stably producing EVs loaded with BRAF^{V600E} nucleic acid drugs (siBRAF^{V600E}). Next, BRAF^{V600E}-mutant and wild-type CRC cell lines, as well as corresponding subcutaneous and metastasis models, were used to evaluate the therapeutic efficacy of EVs-siBRAF^{V600E} and explored the mechanism. Notably, patient-derived xenograft (PDX) models, which share the same molecular characteristics, pathological features, and heterogeneity as patients do, were utilized to further explore the therapeutic efficacy and mechanisms.

Result EVs-siBRAF^{V600E} specifically inhibited BRAF^{V600E} CRC but didn't affect BRAF wild-type CRC in vitro and vivo. EVs-siBRAF^{V600E} exerts its therapeutic effect by regulating the MEK1/2-ERK1/2 pathway, and it has demonstrated excellent therapeutic efficacy in PDX models.

Conclusion The therapeutic EVs we constructed are effective and specific for the BRAF^{V600E}-mutant CRC. This study provides a novel strategy for the treatment of CRC patients with BRAF^{V600E} mutation.

†Di Wang, Liwei Wang and Wei Zhang contributed equally to this work.

*Correspondence:
Wei Zhou
weizhou_srrsh@zju.edu.cn
Xin Liu
xinliuzju@zju.edu.cn
Jianbin Xu
xu9709426@zju.edu.cn

Full list of author information is available at the end of the article

Keywords Colorectal cancer, BRAF^{V600E} mutation, Extracellular vesicles, siRNA, PDX model, Specific therapy

Background

Colorectal cancer (CRC) is one of the most common malignant tumors and is also a heterogeneous disease with subtypes characterized by genetic mutations. Approximately 10-20% of CRC patients harbor BRAF gene mutations, with a portion corresponding to a mutation at codon 600 in exon 15, known as the BRAF^{V600E} mutation [1–6]. With this mutation, the activity of the BRAF gene-encoded product is significantly enhanced compared with that of the wild type, allowing it to continuously promote excessive cell proliferation without the need for cytokine stimulation, thereby inducing tumor development and metastasis [3, 7]. Since CRC patients with the BRAF^{V600E} mutation are insensitive to chemotherapy, their prognosis is very poor, presenting a significant challenge in current clinical treatment [8–10]. Therefore, the treatment of CRC patients with the BRAF^{V600E} mutation is highly important for both basic research and clinical translation.

BRAF, as a member of the RAF family, along with MEK1/2 and ERK1/2, forms the RAF-MEK-ERK (MAPK) signaling pathway, which plays a central role in regulating processes such as cell proliferation, differentiation, cell cycle, and apoptosis [11, 12]. BRAF directly phosphorylates and activates MEK1/2 through its kinase activity and is negatively regulated by the MEK1/2-ERK1/2 feedback loop. BRAF mutations lead to the failure of the MAPK signaling pathway's regulatory mechanisms, resulting in aberrant, sustained activation [13]. The MAPK signaling pathway is a crucial pathway for transmitting extracellular signals, such as those from cytokines, hormones, and cellular stress, into the cell. Dysregulation of this pathway is closely associated with abnormal activation and poor prognosis in various human cancers [11, 12]. Studies have shown that abnormal activation of the MEK1/2-ERK1/2 signaling pathway promotes the proliferation and metastasis of CRC [14, 15]. As the primary signaling pathway activated by BRAF, the MEK1/2-ERK1/2 pathway is also the main mechanism of action for BRAF targeted drugs [16]. Furthermore, the MEK1/2-ERK1/2 pathway is related to resistance to BRAF inhibitors. Reactivation of the MEK1/2-ERK1/2 pathway is one of the primary reasons for BRAF inhibitor resistance. This reactivation is mainly caused by the increased presence of BRAF dimers, which are insensitive to BRAF inhibitors, and feedback regulation leading to upregulation of epidermal growth factor receptor (EGFR) [13, 17]. Combining BRAF inhibitors with MEK or ERK inhibitors is currently the main therapeutic strategy to overcome resistance in patients with BRAF mutations [18].

The standard chemotherapy drugs for treating CRC mainly include 5-FU, irinotecan, and oxaliplatin. These therapies have a median survival time of approximately 17–23 months [19–21]. For CRC patients with the BRAF^{V600E} mutation, the median survival time with first-line chemotherapy is only approximately 11months [9, 10]. Therefore, chemotherapy alone has very limited efficacy for advanced CRC patients with the BRAF^{V600E} mutation. Currently, BRAF inhibitors, such as vemurafenib and encorafenib, have been developed. However, monotherapy with BRAF inhibitors does not yield satisfactory outcomes for patients with BRAF^{V600E} CRC. One study reported that the response rate of BRAF-mutant CRC patients treated with vemurafenib was only 4.8% [22]. In another study, no cases of complete or partial response were observed in advanced BRAF^{V600E} CRC patients treated with encorafenib [23]. The poor efficacy of BRAF inhibitors in CRC is due to their ability to only transiently suppress the phosphorylation of the key kinase MEK1/2. Subsequently, BRAF inhibitors cause rapid feedback activation of epidermal growth factor receptor (EGFR), leading to the bypass of the effects of BRAF inhibitors [17]. Therefore, chemotherapy and BRAF inhibitor monotherapy are not effective in treating CRC with the BRAF^{V600E} mutation.

Gene therapy, such as small interfering RNA (siRNA) drugs, has the potential to achieve breakthroughs in treating tumor subtypes with genetic mutations, such as the BRAF ^{V600E} mutation. However, on the one hand, siRNAs require appropriate delivery vectors to exert their effects. On the other hand, siRNAs can easily lose activity during the complex preparation process. Extracellular vesicles (EVs) are novel drug delivery vehicles derived from cells. Owing to the surface molecules they naturally carry, EVs can evade clearance by the immune system, allowing them to transport drugs over long distances within the body under pathological conditions [24, 25]. EVs not only protect the drugs they carry but also, owing to their endogenous characteristics, enable the delivery of the loaded drugs into cells without disrupting the cell membrane, allowing nucleic acid drugs to perform gene therapy functions [24, 26]. Therefore, by developing cell-derived EV-based therapeutic agents that load nucleic acid drugs, leveraging their drug protection properties and enhancing the permeability and retention (EPR) effect [26, 27], targeted delivery of nucleic acid drugs can be supported.

In this study, we developed a therapeutic system targeting CRC with the BRAF^{V600E} mutation. By preparing engineered cell factories for large-scale production, we obtained a therapeutic agent of EVs that encapsulates

nucleic acid drugs that specifically target the $BRAF^{V600E}$ gene mutation site. This therapeutic system is based on the specific regulation of BRAF-MEK1/2-ERK1/2 signaling pathway activity in tumor cells, providing treatment for CRC with the $BRAF^{V600E}$ mutation. We validated the therapeutic efficacy and mechanism of action of this therapeutic system through CRC cell line-derived xenograft (CDX) models, metastasis models, and patient-derived xenograft (PDX) models (Fig. 1). We explored an effective treatment strategy for CRC with the $BRAF^{V600E}$ mutation, which also has potential for application in the treatment of other tumors with the $BRAF^{V600E}$ mutation, such as malignant melanoma and thyroid cancer.

Method

Cell culture and tissues

CRC cell lines, including RKO, HCT116, COLO320, and HT29, were purchased from the American Type Culture Collection (Manassas, VA, USA). Human embryonic kidney cells (HEK293T) were purchased from the Cell Bank of the Shanghai Academy of Chinese Sciences. The mutational status of the cell lines used in this study can be obtained from the Cancer Cell Line Encyclopedia database and a previous study. All the cell lines were maintained in Dulbecco's modified essential medium (DMEM) or McCoy's 5 A medium (Gibco BRL, Rockville, MD) supplemented with 100 μg/mL streptomycin, 100 U/mL penicillin and 10% fetal bovine serum (FBS; Gibco, NY, USA) and incubated at 37 °C in a 5% humidified CO_2 atmosphere. The CRC tissues from the patients included in this study were obtained from surgical resection specimens of CRC patients treated at Sir Run Run Shaw Hospital (Hangzhou, Zhejiang, China), Zhejiang University, during the year 2024. This study was approved and monitored by the Ethics Committee of Sir Run Run

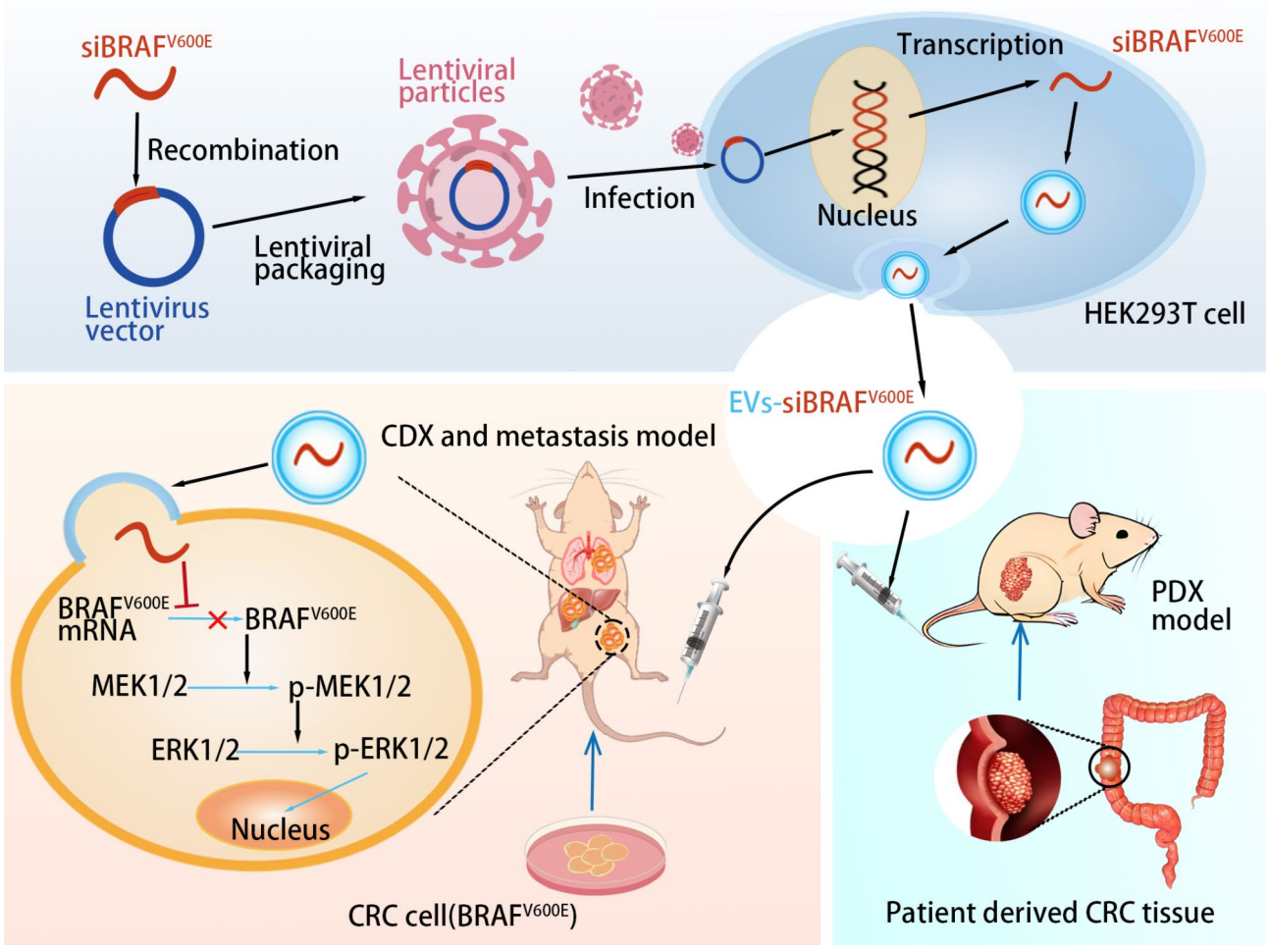

Fig. 1 Schematic illustration of the therapeutic system based on EVs used for the delivery of nucleic acid drugs targeting gene mutation sites for the precise treatment of CRC with the $BRAF^{V600E}$ mutation. $siBRAF^{V600E}$ was transfected into HEK293T cells via a lentiviral vector to stably produce EVs carrying $siBRAF^{V600E}$. After treatment with these EVs- $siBRAF^{V600E}$, the BRAF-MEK1/2-ERK1/2 pathway was inhibited in CRC cells. Subcutaneous xenograft tumor models and metastasis models of CRC cell lines were used to validate the therapeutic effects and toxicity of the EVs-$siBRAF^{V600E}$. The efficacy of the EVs-$siBRAF^{V600E}$ was further confirmed via PDX models

Shaw Hospital, Zhejiang University (Acceptance Number: 2024-2450-01).

shRNA lentiviral construction and stably infected cell cultivation

The siRNA sequence targeting the $BRAF^{V600E}$ mutation is 5'-GCU ACA GAG AAA UCU CGA U-3'. This sequence was subsequently cloned and inserted into a lentiviral vector to construct a shRNA vector. Lentivirus production was performed with a Lenti-Pac HIV package kit and Lipofectamine 3000 (Invitrogen, CA, USA) according to the manufacturers' instructions. After transfection, stable HEK293T, RKO and COLO320 cells were selected with puromycin (Gibco, Grand Island, NY, USA) for several days, and the surviving cells were continuously cultured as stable cells.

RNA extraction and quantitative real-time PCR (qRT-PCR)

Total RNA was extracted from cells and extracellular vesicles via TRIzol reagent (Invitrogen) according to the manufacturer's instructions. mRNA reverse transcription (RT) via an Evo M-MLV RT Master Mix Kit (Accurate Biotechnology, China), and siRNA RT via a miRNAFirst Strand cDNA Synthesis (Stem-loop Method) Kit (Sango Biotech, China). Quantitative PCR (qPCR) were performed via a Hieff qPCR SYBR Green Master Mix Kit (Yeasen Biotechnology, China) according to the manufacturers' instructions. Typically, amplification reactions were performed in a 10 μL reaction system containing 2× SYBR Green Premix, a 0.2 μM primer mixture and moderate cDNA diluted with ddH_2O. The thermal cycling profiles for qRT-PCR included heating at 95 °C for 30 s followed by 40 cycles at 95 °C for 5 s and 60 °C for 30 s, and the cDNA copy number was monitored via quantitative analysis of fluorescence emissions via a Roche LightCycler 480 II PCR instrument (Basel, Switzerland). The threshold cycle (Ct) represents the refraction cycle number at which a positive amplification reaction was measured. Glyceraldehyde-3-phosphate dehydrogenase (GAPDH) was used as an internal standard control. The primer sequences used are shown in Supplementary Table 1. Expression was quantified via the $2^{-\Delta\Delta ct}$ method.

Isolation and identification of extracellular vesicles

HEK293T cell culture media were harvested and centrifuged at 300× g and 3,000× g to remove cells and debris first. The supernatant was subsequently centrifuged at 10,000× g for 30 min, and larger shedding vesicles were discarded. Then, the supernatant was centrifuged at 110,000× g for 70 min and the pellet was retained. Finally, the pellet was washed with PBS and centrifuged at 110,000× g for 70 min again. EVs were contained in the pellet, which was resuspended in PBS. All steps were performed at 4 °C. A BCA protein assay kit (Beyotime, China) was used to determine the extracellular vesicle concentration. Nanoparticle tracking analysis (NTA) with a Zetasizer Nano (Malvernpanalytical, U.K.) and transmission electron microscopy (TEM) (JEOL, Japan) were used to identify EVs.

Measurement of EVs uptake in vitro and biodistribution in vivo

For EVs uptake in vitro, EVs were labeled with DiD (Beyotime, Shanghai, China), and cells were cultured with DiD-labeled EVs for 24 h. Then, the cells were washed thrice with PBS, fixed with 4% paraformaldehyde, and stained with DAPI (Beyotime, Shanghai, China). The cellular uptake of EVs was observed under a fluorescence microscope (Leica, Germany).

To determine in vivo distribution of EVs, mice were intravenously injected with DiD-labeled EVs. After 24 h of intravenous injection, DiD fluorescence signals in the dissected tumor and organs (heart, liver, spleen, lung and kidneys) were captured using a spectrum in vivo imaging system (IVIS) (PerkinElmer, USA).

Western blotting (WB)

The cells were placed in a 6-well plate (1×10^6 cells per well) for 24 h. Then, the cells were treated with 2 mL of fresh complete medium supplemented with PBS, EVs-NC, or EVs-$siBRAF^{V600E}$ for 24 h (the concentration of the extracellular vesicles was 50 μg/mL). After that, the cells were harvested for Western blot analysis as follows. The treated cells were washed with PBS and lysed in RIPA lysis buffer with phosphatase inhibitor cocktail and protease inhibitor cocktail (Sigma-Aldrich, Germany). The lysate samples were subsequently centrifuged at 12,000 × g for 15 min at 4 °C. A BCA protein assay kit (Beyotime, China) was subsequently used to determine protein concentrations. Next, all the samples were electrophoresed through a 10% Bis-Tris polyacrylamide gel. After that, the protein in the gel was transferred to a 0.45 μm polyvinylidene fluoride (PVDF) membrane (Millipore, USA). The PVDF membranes were blocked with TBST buffer containing 5% skim milk powder and incubated with the corresponding primary antibodies at 4 °C overnight. The primary antibodies used were against BRAF (ab33899, Abcam), MEK1/2 (11049-1-AP, Proteintech), phospho-MEK1/2 (p-MEK1/2) (9154s, Cell Signaling Technology), p44/42 MAPK (ERK1/2) (4695s, Cell Signaling Technology), phospho-p44/42 MAPK (p-ERK1/2) (4370s, Cell Signaling Technology), GAPDH (2118s, Cell Signaling Technology), TSG101 (ab125011, Abcam), CD81 (ab109201, Abcam) and CD63 (ab134045, Abcam). The membrane was subsequently hybridized with an HRP-conjugated secondary antibody (D110058 and D110087; Sangon Biotech, China) for 60 min at room temperature with gentle rocking. An imaging system (GE, USA) with

a chemiluminescent ECL substrate (FD8030, Fudebio, China) was used to detect fluorescence signals on the PVDF membranes, and grayscale values were quantified via ImageJ.

Cell-counting Kit-8(CCK-8) assay

For cell viability, RKO, HT29, HCT116 and COLO320 cells were cultured in complete medium containing PBS, EVs-NC or EVs-siBRAF^{V600E} for 5 days. The concentrations of EVs-NC and EVs-siBRAF^{V600E} were 50 μg/mL. Every day, the cells were incubated with fresh medium containing 10% Cell-Counting Kit-8 solution (Boster Bio, China) per well for 1 h. A microplate reader (Bio-Rad 680, USA) was used to measure the optical density of the mixture at 450 nm.

Wound-healing assay

Cell motility was assessed via a scratch wound assay. The cells were cultured in medium containing 10% FBS in 6-well plates. When the cells reached 100% confluence, the cell monolayer was subsequently scratched with a 10 μL pipette tip. The cells were washed twice with PBS and treated with 2 mL of fresh 1% FBS medium supplemented with PBS, EVs-NC, or EVs-siBRAF^{V600E} for 24 h (the concentration of the extracellular vesicles was 50 μg/mL). The wounds were photographed under a microscope. The width of wound healing was quantified and compared with baseline values, and the results were expressed as the percentage of wound-healing. The wound-healing percentage was calculated as the migration distance/scratch width×100%. Specifically, the migration distance equals the width at which the cell migrated over 24 h. The scratch width represents the distance at which the scratch was made at 0 h.

EdU assay

The cells were placed in 24-well plates (2×10^5 cells per well) with 0.5 mL of complete medium for 24 h. After that, the cells were treated with 0.5 mL of fresh complete medium supplemented with PBS, EVs-NC, or EVs-siBRAF^{V600E} for 48 h (the concentration of extracellular vesicles was 50 μg/mL). Then, the cells were fixed with 4% polymethanol for 20 min. Next, the cells were stained with a Cell-Light EdU In Vitro Kit (Ribobio, China) according to the manufacturers' instructions. Images were acquired via fluorescence microscopy (Eclipse E6000; Nikon, Japan).

Flow cytometric analysis of apoptosis

The cells were placed in 6-well plates (5×10^5 cells per well) with 2 mL of complete medium for 24 h. After that, the cells were treated with 2 mL of fresh complete medium supplemented with PBS, EVs-NC or EVs-siBRAF^{V600E} for 24 h (the concentration of extracellular vesicles was 50 μg/mL). The cells were subsequently harvested with EDTA-free trypsin. Finally, the cells were stained with an Annexin V-FITC/PI apoptosis kit (MultiSciences, China) according to the manufacturers' instructions, and detected with a DxFLEX flow cytometer (Beckman, USA).

Animal model

All the animal experiments were reviewed and approved by the Laboratory animal management and ethics committee of the Second Affiliated Hospital, Zhejiang University School of Medicine (approval number: 2024 – 170). Human CRC cell-derived tumor xenograft models were developed via the subcutaneous injection of RKO cells (2×10^5 cells in 100 μL per mouse) into the left flank of female BALB/c nude mice. When the volume of tumors reached approximately 100 mm^3(approximately 7 days), 20 μg of different EVs (resuspended in 50 μL of PBS) or PBS was injected intravenously through the tail vein every 3 days. The volume of the tumors was measured and calculated every 3 days according to $\pi/6\times(\text{length}\times\text{width}^2)$. After treatment, the animals were sacrificed, and major organs, blood and tumor tissues were collected for further analysis. Lung and liver metastasis models of human CRC were developed by injecting 2×10^5 RKO cells labeled by luminescence into the tail vein and spleen of female BALB/c nude mice, respectively. After the cells were injected for 7 days, 20 μg of different EVs (resuspended in 50 μL of PBS) or PBS was injected intravenously through the tail vein every 3 days. To image the tumors in live animals, the mice were anesthetized with isoflurane and intraperitoneally injected with 150 mg/kg D-luciferin (Yeason, China). After 15 min, the tumor cells labeled by luminescence were imaged via a Spectrum in vivo imaging system (IVIS) (PerkinElmer, USA).

PDX model

This study involving human tumor tissues was approved by the institutional Ethics Committee of Sir Run Run Shaw Hospital, Zhejiang University. Fresh human cancer tissues were cut into approximately 1-3mm^3 pieces and placed in the left flank of female BALB/c nude mice. When the volume of tumors reached approximately 100 mm^3, 20 μg of different EVs (resuspended in 50 μL of PBS) or PBS was injected intravenously through the tail vein every 3 days. The volume of tumors was measured and calculated every 3 days according to $\pi/6\times(\text{length}\times\text{width}^2)$. Then, the animals were subsequently sacrificed, and tumor tissues were collected for further analysis.

Histological analysis

The tumor tissues were fixed in 4% neutral buffered formalin for immunohistochemical (IHC) staining. To block endogenous peroxidase activity, the paraffin embedded tissue sections were incubated with 0.3% H_2O_2 for 30 min at room temperature. Then, 10% goat serum was used to block the sections for 30 min at room temperature. Next, the sections were incubated with different primary antibodies overnight at 4 °C. The primary antibodies used were against $BRAF^{V600E}$ (ZA-0668, ZSGB-BO, China), KI67 (27309-1-AP, Proteintech), BRAF (ab33899, Abcam), and phospho-p44/42 MAPK (p-ERK1/2) (4370s, Cell Signaling Technology). Then, the sections were washed with PBS. After that, the sections were incubated with secondary antibody for 1 h at room temperature. Finally, the sections were observed via a microscope.

Statistical analysis

The data were presented as the means ± standard deviations. Data in two groups were compared by two-tailed Student's t-tests. The repeated measures ANOVA (Two-way ANOVA) was used to analyze CCK-8 assays and tumor volume changes in vivo. One-way ANOVA followed by Tukey test multiple comparisons was used to compare data in multiple groups. GraphPad Prism 8 software was used for statistical analysis. The experimental group was the independent factor. Statistical significance was set at $^{*}p < 0.05$, $^{**}p < 0.01$, and $^{***}p < 0.001$.

Results

BRAF mutation is a poor prognostic factor in CRC

We used public databases to explore the relationship between BRAF mutation and prognosis in CRC patients. First, we utilized the cBioPortal database (https://www.cbioportal.org/) to analyze the survival data of bowel tumor patients. We selected all patients with bowel tumors from studies included in the database and grouped them on the basis of BRAF mutation status (wild type, WT; mutant type, MT). As shown in Fig. 2A, the analysis revealed that among 3,883 patients, the median overall survival (OS) (95% CI) for BRAF-mutant ($BRAF^{MT}$) patients was 45.50 months (37.02–67.30), whereas for BRAF wild-type ($BRAF^{WT}$) patients, it was 65.80 months (59.93–72.48), indicating that $BRAF^{MT}$ patients have shorter survival times. Subsequently, we performed multivariate Cox proportional hazards regression analysis via CVCDAP website (https://omics.bjcancer.org/cvcdap/single_survivalanalysis.do) to assess the prognosis of colon cancer patients in the TCGA database. As shown in Fig. 2B, both BRAF mutation and stage IV were poor prognostic factors in colon cancer patients. To further investigate the relationship between BRAF and survival in patients with BRAF mutation, we conducted survival analysis using the Kaplan-Meier Plotter website (https://kmplot.com/analysis/index.php?p=background) on colon cancer data from the TCGA database. As shown in Fig. 2C, among 53 colon cancer patients with BRAF mutations, those with high BRAF mRNA levels had shorter recurrence-free survival (RFS) than did those with low BRAF mRNA levels. These findings suggested that high BRAF expression is also a poor prognostic factor in patients with $BRAF^{MT}$ colon cancer.

To further analyze the impact of $BRAF^{V600E}$ on the prognosis of CRC patients, we collected tissue samples from CRC patients with either $BRAF^{WT}$ or $BRAF^{V600E}$ and performed IHC analysis of KI67 positivity. KI67 is a commonly used clinical marker for assessing tumor proliferative activity and predicting patient prognosis. As shown in Fig. 2D and E, $BRAF^{V600E}$ patients had a higher KI67 positivity rate than $BRAF^{WT}$ patients did. On the basis of our analysis of public data and our clinical specimens, we concluded that the BRAF mutation is a poor prognostic factor in CRC patients.

Construction and characterization of therapeutic agents for the $BRAF^{V600E}$ mutation

We used a specific siRNA sequence, $siBRAF^{V600E}$ (5'-GCU ACA GAG AAA UCU CGA UTT-3'), to target the $BRAF^{V600E}$ mutation site. First, we used this sequence to construct shRNA lentiviral vectors. To verify the specificity of $siBRAF^{V600E}$ for the $BRAF^{V600E}$ mutation, we infected the $BRAF^{V600E}$ mutant CRC cell line RKO and the wild-type BRAF ($BRAF^{WT}$) CRC cell line COLO320 with the shRNA lentivirus. Through quantitative real-time PCR (qRT-PCR) analysis, we found that BRAF mRNA levels in COLO320 and HEK293T cells did not significantly decrease, whereas BRAF mRNA levels decreased in RKO cells (Fig. 3A). As shown in Fig. 3B, we infected HEK293T cells with $BRAF^{V600E}$-specific shRNA lentivirus to obtain engineered cells stably expressing $siBRAF^{V600E}$, which were used to stably generate therapeutic extracellular vesicles carrying $siBRAF^{V600E}$ ($EVs\text{-}siBRAF^{V600E}$). Correspondingly, negative control lentiviral infection of HEK293T cells was performed to obtain negative control extracellular vesicles(EVs-NC). We separately extracted EVs-NC and $EVs\text{-}siBRAF^{V600E}$, and the particle sizes of EVs-NC and $EVs\text{-}siBRAF^{V600E}$ were similar (Fig. 3C), with both exhibiting a discoidal or cup-shaped morphology (Fig. 3D, E) via NTA analysis and transmission electron microscopy. We extracted proteins from EVs-NC and $EVs\text{-}siBRAF^{V600E}$ and found through Western blotting that both expressed the extracellular vesicle marker molecules TSG101, CD81, and CD63 (Fig. 3F). After EVs-NC and $EVs\text{-}siBRAF^{V600E}$ were labeled with DiD, we coincubated them with RKO cells and observed via fluorescence microscopy that RKO cells were able to take up both EVs-NC and $EVs\text{-}siBRAF^{V600E}$ (Fig. 3G).

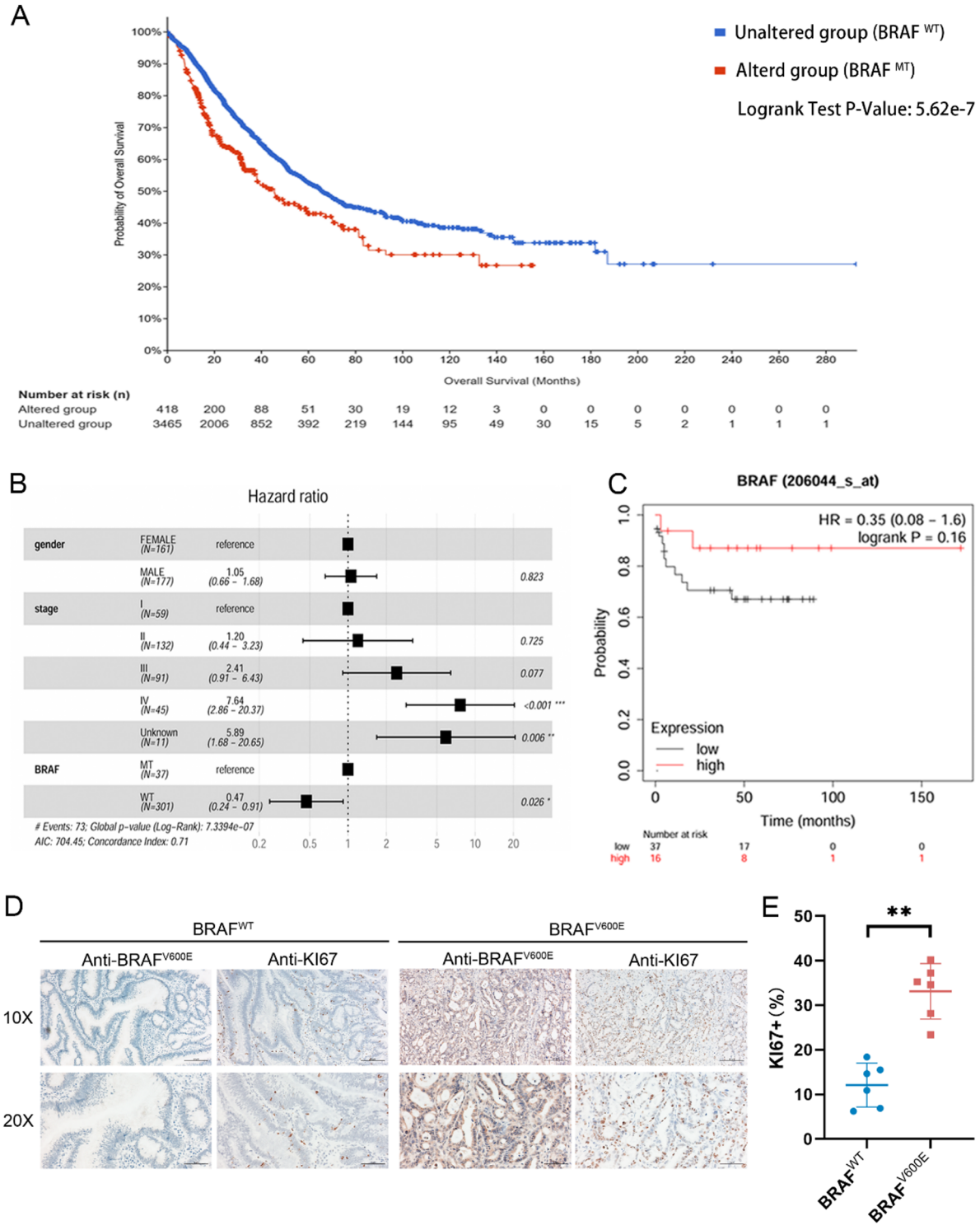

Fig. 2 BRAF mutation is a poor prognostic factor in CRC patients. (**A**) K-M survival curves of patients with BRAF mutation and wild-type CRC. (**B**) Multivariate COX regression model analysis of gender, stage and BRAF mutation status in CRC patients. (**C**) K-M survival curve of BRAF expression level in $BRAF^{MT}$ CRC. (**D**) Representative IHC images of $BRAF^{V600E}$ and KI-67 in CRC tissues. The scale bar represents 10 μm for the 10x objective and 5 μm for the 20x objective. (**E**) KI67 positivity rate in CRC tissues with $BRAF^{V600E}$ or $BRAF^{WT}$. The data are reported as the means ± SDs of the experiments ($n = 3$). Two-tailed Student's t-tests, $^{**}p < 0.01$

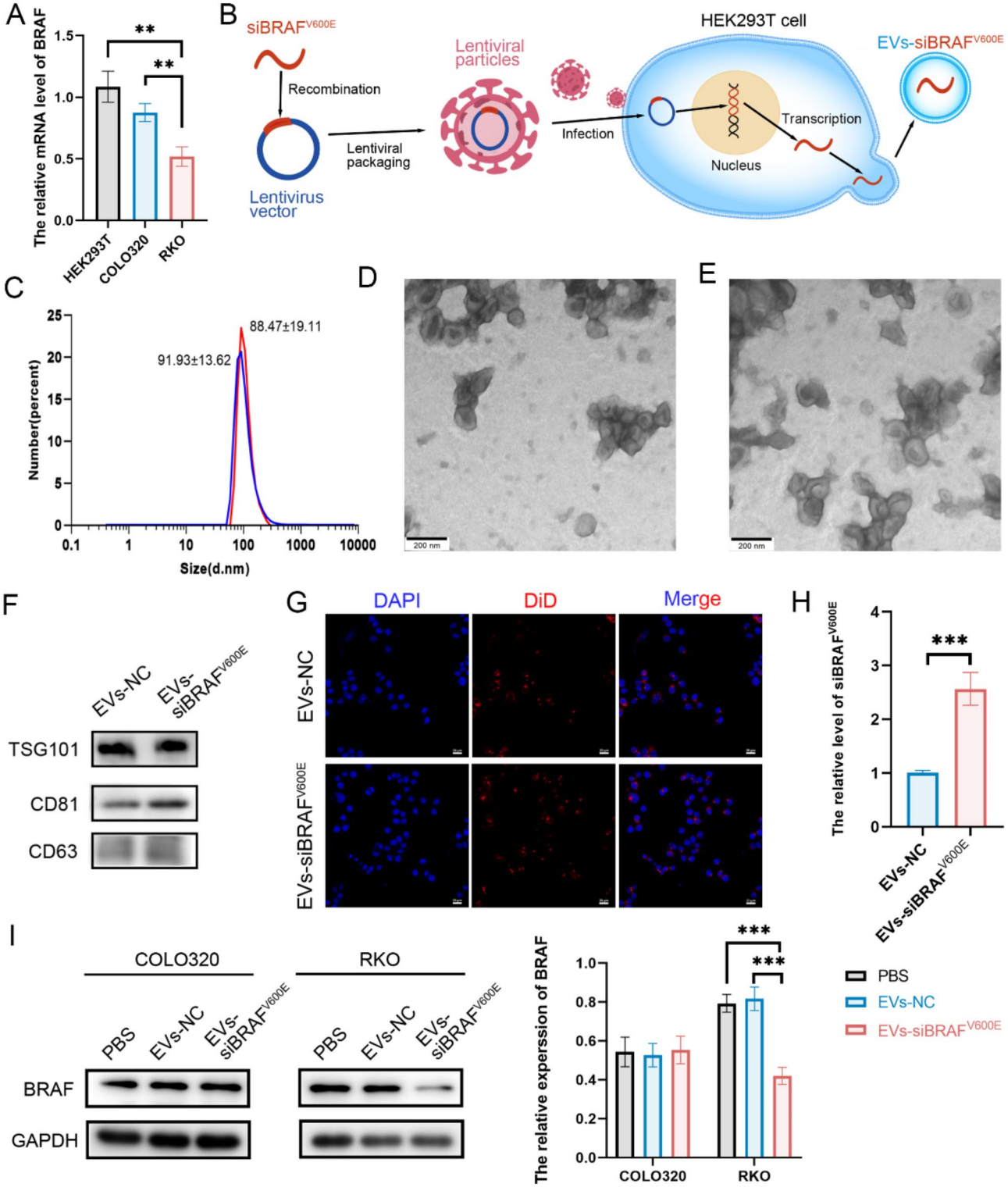

Fig. 3 Construction and characterization of EVs-siBRAF^{V600E}. (**A**) BRAF mRNA levels were analyzed by qRT-PCR. BRAF mRNA levels were measured after treating HEK293T, COLO320, and RKO cells with 50 μg/mL of EVs-siBRAF^{V600E} for 24 h. (**B**) Construction of the therapeutic agent. (**C**) NTA analysis of EVs-NC (blue) and EVs-siBRAF^{V600E} (red). (**D**)(**E**) TEM images of eVs-NC (**D**) and EVs-siBRAF^{V600E} (**E**); scale bar: 200 nm. (**F**) WB analysis of the extracellular vesicle marker proteins, TSG101, CD81 and CD63. (**G**) Fluorescence microscopy images showing the uptake of EVs-NC and EVs-siBRAF^{V600E} by RKO cells. The cell nuclei were stained with DAPI, and the EVs were stained with DiD; scale bar: 20 μm. (**H**) qRT-PCR analysis of siBRAF^{V600E} levels in EVs-NC and EVs-siBRAF^{V600E}. (**I**) WB analysis of BRAF protein levels. After COLO320 and RKO cells were treated with PBS, or 50 μg/mL of EVs-NC or EVs-siBRAF^{V600E} for 24 h, cell proteins were extracted to measure BRAF protein expression. The data are reported as the means ± SDs of the experiments ($n = 3$). Two-tailed Student's t-tests for (**a**) and (**h**), and one-way ANOVA followed by Tukey test multiple comparisons for (**I**), $^{*}p < 0.05$, $^{**}p < 0.01$ and $^{***}p < 0.001$

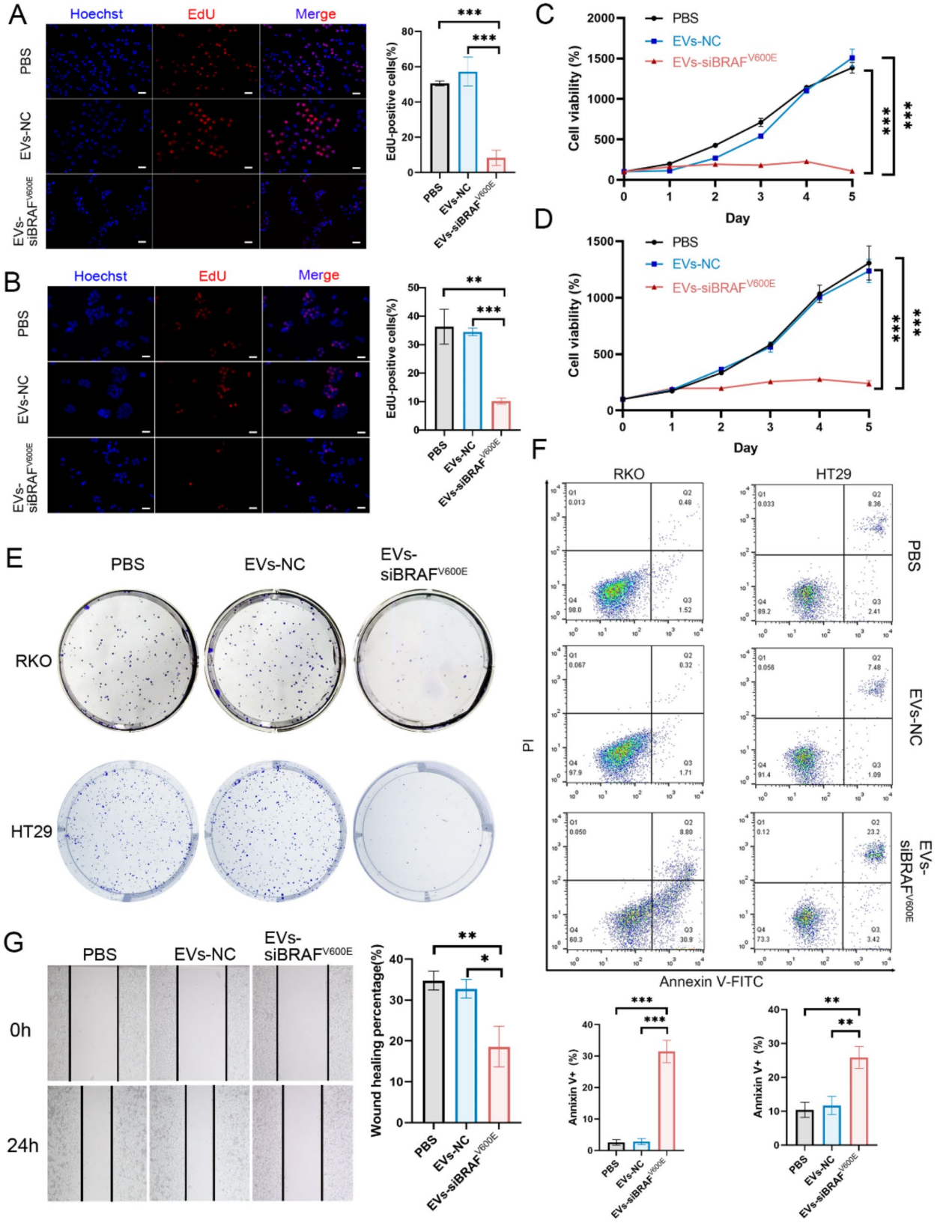

Fig. 4 (See legend on next page.)

(See figure on previous page.)

Fig. 4 EVs-siBRAF^{V600E} can inhibit BRAF^{V600E} CRC cells. RKO (**A**) and HT29 (**B**) cells were treated with PBS, EVs-NC or EVs-siBRAF^{V600E} for 48 h, followed by EdU assays to measure cell proliferation activity and imaging via fluorescence microscopy. Scale bar: 20 μm. RKO(**C**) and HT29 (**D**) cells were treated with PBS, EVs-NC or EVs-siBRAF^{V600E} for 5 days, and cell viability was measured via CCK-8 assays. (**E**) Colony formation. Images of single-cell-derived colonies formed by RKO and HT29 cells after treatment with PBS, EVs-NC or EVs-siBRAF^{V600E} for 2 weeks. (**F**) Flow cytometry analysis of cell apoptosis. RKO and HT29 cells were treated with PBS, EVs-NC or EVs-siBRAF^{V600E} for 24 h, stained with Annexin V-FITC and PI, and apoptosis was detected via flow cytometry. (**G**) Cell migration was assessed by wound healing assays. RKO cells were treated with PBS, EVs-NC or EVs-siBRAF^{V600E} for 24 h. The concentration of EVs-NC or EVs-siBRAF^{V600E} in all the treatments was 50 μg/mL. The data are reported as the means ± SDs of the experiments ($n = 3$). Two-way ANOVA for (**A**) and (**B**), and one-way ANOVA followed by Tukey test multiple comparisons for the others, *$p < 0.05$, **$p < 0.01$ and ***$p < 0.001$

Extracellular vesicles were extracted from HEK293T cells, and RNA was extracted from the extracellular vesicles for qRT-qPCR analysis, revealing a significant increase in siBRAF^{V600E} levels in EVs-siBRAF^{V600E} (Fig. 3H). Treatment of the CRC cell lines COLO320 and RKO with PBS and extracellular vesicles derived from HEK293T cells, EVs-siBRAF^{V600E} resulted in decreased BRAF levels in RKO cells, whereas there was no significant effect on BRAF levels in COLO320 cells (Fig. 3I). The above results demonstrated that the therapeutic extracellular vesicles we constructed can carry siRNAs targeting the BRAF^{V600E} mutation and effectively reduce BRAF levels in colorectal cancer cells with the BRAF^{V600E} mutation, without affecting BRAF levels in BRAF^{WT} colorectal cancer cells. Furthermore, the methods we used to construct and extract therapeutic EVs do not significantly affect the properties of the EVs.

Inhibitory effects of therapeutic agents in BRAF^{V600E}-mutant CRC in vitro

After we obtained the therapeutic agent that can stably produce the targeted BRAF^{V600E} mutation, we selected the CRC lines RKO and HT29, which have the BRAF^{V600E} mutation. When RKO and HT29 cells were treated with EVs-NC or EVs-siBRAF^{V600E}, respectively, an EdU assay confirmed a significant decrease in the proliferative activity of RKO and HT29 cells treated with EVs-siBRAF^{V600E} compared with those in the PBS and EVs-NC groups (Fig. 4A, B). Further validation through CCK-8 assays revealed that the proliferation of cells treated with EVs-siBRAF^{V600E} was significantly inhibited compared with that of those treated with PBS, whereas there was no significant difference between the EVs-NC and the PBS treatment group (Fig. 4C, D). After treating RKO and HT29 cells with EVs-NC or EVs-siBRAF^{V600E} for 2 weeks, significantly fewer colonies formed in the EVs-siBRAF^{V600E} group than in the PBS and EVs-NC groups, with almost no observable colony formation, while there was no significant difference between the EVs-NC and PBS treatment groups (Fig. 4E). Similarly, flow cytometry analysis of apoptosis in RKO and HT29 cells treated with both types of EVs for 24 h revealed a significant increase in apoptosis in cells treated with EVs-siBRAF^{V600E} compared with those treated with PBS, whereas no significant increase in apoptosis was observed in cells treated with EVs-NC (Fig. 4F). These results indicated that EVs-siBRAF^{V600E} significantly inhibited proliferation and promoted apoptosis in BRAF^{V600E}-mutant CRC cells.

Furthermore, we utilized wound-healing assays to observe the effect of EVs-siBRAF^{V600E} on tumor cell migration. We found that after 24 h of treatment with EVs-siBRAF^{V600E}, the migratory ability of RKO cells was significantly reduced (Fig. 4G). Owing to the inherently weak migratory ability of HT29 cells, no significant difference was observed (data not shown). The above results demonstrated that our therapeutic agent significantly suppressed the viability and metastasis of colorectal cancer cells with BRAF^{V600E} mutation.

Inhibitory effects of therapeutic agents on BRAF^{WT} CRC in vitro

To observe the specificity of the therapeutic extracellular vesicles we constructed targeting the BRAF^{V600E} mutation, we selected the BRAF^{WT} colorectal cancer cell lines COLO320 and HCT116. After treating the tumor cells with EVs-NC and EVs-siBRAF^{V600E}, we found that the proliferation of COLO320 and HCT116 cells treated with EVs-siBRAF^{V600E} was not inhibited compared with the PBS treatment group, and there was no significant difference compared with the EVs-NC treatment group as well via CCK-8 assays (Fig. 5A, B). Further validation through EdU assays confirmed that EVs-siBRAF^{V600E} treatment did not affect the proliferation of COLO320 and HCT116 cells (Fig. 5C, D). After treating COLO320 and HCT116 cells with EVs-siBRAF^{V600E} and EVs-NC for 2 weeks, we found that the formation of colonies in both the EVs-NC and EVs-siBRAF^{V600E} treatment groups did not significantly differ from that in the PBS group (Fig. 5E). These experimental results indicated that EVs-siBRAF^{V600E} did not inhibit the proliferation of BRAF^{WT} colorectal cancer cells.

After COLO320 and HCT116 cells were treated with extracellular vesicles for 24 h, flow cytometry analysis revealed that apoptosis did not increase in cells treated with EVs-siBRAF^{V600E} compared with those in the PBS and EVs-NC groups (Fig. 5F). Wound-healing assays were used to observe the effect of EVs-siBRAF^{V600E} on tumor cell migration, and 24 h after treatment, the migratory ability of COLO320 and HCT116 cells was not reduced compared with that of the PBS and EVs-NC groups (Fig. 5G). The above results demonstrated that our therapeutic agent did not significantly affect the behavior of

colorectal cancer cells with $BRAF^{WT}$, and indicating that it specifically interferes with the $BRAF^{V600E}$ mutation.

The inhibitory effect of therapeutic agents is mediated by the BRAF-MEK1/2-ERK1/2 signaling pathway

Furthermore, we explored the mechanism of this therapeutic agent. First, we detected the mRNA levels of BRAF by qRT-PCR after treatment. After RKO and HT29 cells were treated with EVs, the mRNA levels of BRAF in the EVs-si$BRAF^{V600E}$ group were significantly lower than those in the PBS and EVs-NC groups (Fig. 6A, B). We then examined the protein levels of BRAF and the phosphorylation levels of MEK1/2 and ERK1/2 through Western blotting. After RKO and HT29 cells were treated with PBS or EVs, the protein levels of BRAF in the EVs-si$BRAF^{V600E}$ group were significantly lower than those in the PBS and EVs-NC groups (Fig. 6C, D). Moreover, compared with those in the PBS and EVs-NC groups, the phosphorylation levels of MEK1/2 and ERK1/2 in the EVs-si$BRAF^{V600E}$ treatment group were also significantly lower (Fig. 6C, D). These results demonstrated that EVs-si$BRAF^{V600E}$ treatment can reduce the activity of the BRAF-MEK1/2-ERK1/2 signaling pathway in $BRAF^{V600E}$-mutant CRC cells, thereby inhibiting tumor cells.

In the above experiments, we found that EVs-si$BRAF^{V600E}$ had no significant effect on $BRAF^{WT}$ CRC cells. To further verify that EVs-si$BRAF^{V600E}$ specifically target $BRAF^{V600E}$ and regulate the BRAF-MEK1/2-ERK1/2 pathway, we examined the activity levels of the BRAF-MEK1/2-ERK1/2 pathway in the $BRAF^{WT}$ CRC cell lines, COLO320 and HCT116, after EVs treatment. As shown in Fig. 6E and F, there was no significant difference in BRAF mRNA or protein levels between the EVs-si$BRAF^{V600E}$ treatment group and the EVs-NC or PBS groups. Detection of the phosphorylation levels of MEK1/2 and ERK1/2 revealed that there was also no significant difference between the EVs-si$BRAF^{V600E}$ group and the EVs-NC or PBS groups (Fig. 6G, H).

BRAF has been reported to activate downstream MEK1/2 activity through phosphorylation, and activated MEK1/2 can phosphorylate downstream ERK1/2, leading to the generation of active ERK1/2, which performs transcription factor functions [7, 28]. In normal cells, the activity of BRAF is regulated by upstream RAS [28]. However, in tumor cells with the $BRAF^{V600E}$ mutation, the mutated BRAF is persistently activated, leading to continuous activation of the BRAF-MEK1/2-ERK1/2 signaling pathway, thereby promoting tumor cell growth [3, 7]. The above experimental results revealed that the specific therapeutic extracellular vesicles we constructed, EVs-si$BRAF^{V600E}$, can inhibit $BRAF^{V600E}$-mutant CRC cells but have no significant effect on $BRAF^{WT}$ CRC cells. Our therapeutic agent can specifically inhibit the BRAF-MEK1/2-ERK1/2 signaling pathway in $BRAF^{V600E}$ CRC cells, thereby suppressing tumor cell behaviors and functions (Fig. 6I), without affecting the activity of the BRAF-MEK1/2-ERK1/2 signaling pathway in $BRAF^{WT}$ CRC cells.

Inhibitory effects of therapeutic agents in $BRAF^{V600E}$-mutant CRC in vivo

As shown in Fig. 7A, we established a subcutaneous CRC model by injecting RKO cells into BALB/c nude mice subcutaneously. When the tumors reached approximately 100 mm^3 in size (7 days after cell injection), the mice were randomly divided into 3 groups and intravenously injected with PBS, EVs-NC, or EVs-si$BRAF^{V600E}$ every 3 days for a total of 8 injections. 3 days after the last treatment, the mice were euthanized, and the tumors were extracted. We observed that the tumor volume in the mice treated with EVs-si$BRAF^{V600E}$ grew significantly slower than that in the PBS and EVs-NC treatment groups (Fig. 7B). Upon euthanasia, the tumors were weighed, revealing that the tumors in the EVs-si$BRAF^{V600E}$ treatment group were significantly smaller than those in the PBS and EVs-NC groups were (Fig. 7C, D). IHC analysis of tumor tissues was performed to detect BRAF expression and ERK1/2 phosphorylation levels. As shown in Fig. 7E, compared with the PBS and EVs-NC groups, the EVs-si$BRAF^{V600E}$ treatment group presented lower levels of BRAF expression and ERK1/2 phosphorylation in the tumors. To further analyze the activity of the BRAF-MEK1/2-ERK1/2 signaling pathway in tumor tissues, we extracted proteins from tumor tissues. Western blotting was performed to measure BRAF expression levels and MEK1/2 and ERK1/2 phosphorylation levels. Compared with the PBS and EVs-NC groups, the EVs-si$BRAF^{V600E}$ treatment group presented lower levels of BRAF expression and significantly lower phosphorylation levels of MEK1/2 and ERK1/2 in the tumors (Fig. 7F-I). These results indicated that our therapeutic agent can inhibit the growth of $BRAF^{V600E}$ CRC in vivo and reduce the activity of the BRAF-MEK1/2-ERK1/2 signaling pathway in tumors.

To investigate whether our therapeutic agent, EVs-si$BRAF^{V600E}$, can inhibit tumor metastasis, we established BALB/c nude mouse models of CRC lung metastasis and liver metastasis via intravenous injection and splenic injection of RKO cells. One week later, the mice were randomly divided into 3 groups and intravenously injected with PBS, EVs-NC, or EVs-si$BRAF^{V600E}$ every 3 days for a total of 8 injections. 3 days after the last treatment, the sizes of the lung and liver metastases were observed. As shown in Fig. 7J and K, the lung and liver metastases in the mice treated with EVs-si$BRAF^{V600E}$ were significantly smaller than those in the PBS and EVs-NC groups. These results demonstrated that the

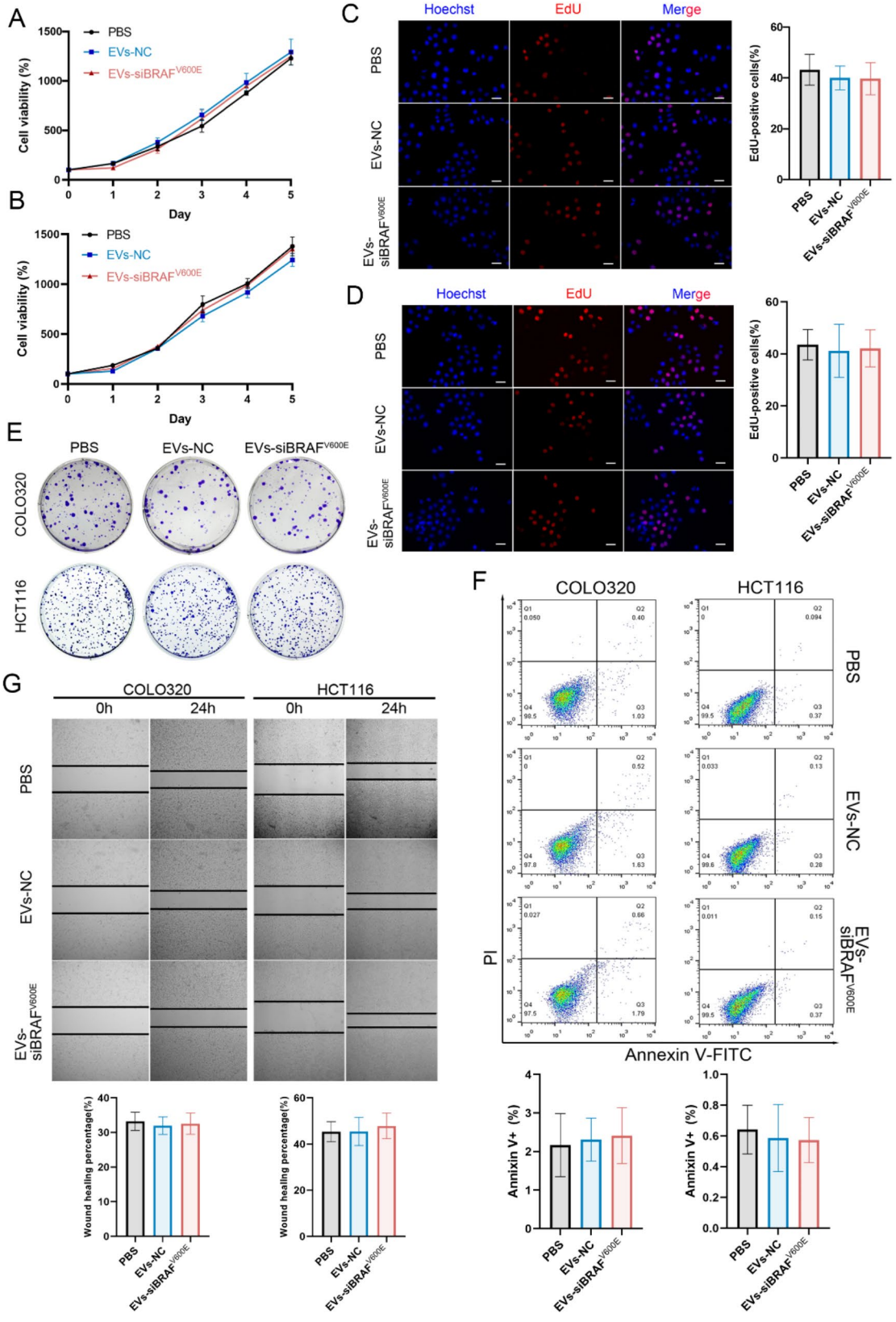

Fig. 5 (See legend on next page.)

(See figure on previous page.)

Fig. 5 EVs-siBRAF^{V600E} cannot inhibit BRAF^{WT} CRC cells. COLO320(**A**) and HCT116 (**B**) cells were treated with PBS, EVs-NC or EVs-siBRAF^{V600E} for 5 days, and cell viability was measured via CCK-8 assays. COLO320(**C**) and HCT116 (**D**) cells were treated with PBS, EVs-NC or EVs-siBRAF^{V600E} for 48 h, followed by EdU assays to measure cell proliferation activity and imaging using fluorescence microscopy. Scale bar: 20 μm. (**E**) Colony formation. Images of single-cell-derived colonies formed by COLO320 and HCT116 cells after treatment with PBS, EVs-NC or EVs-siBRAF^{V600E} for 2 weeks. (**F**) Flow cytometry analysis of cell apoptosis. COLO320 and HCT116 cells were treated with PBS, EVs-NC or EVs-siBRAF^{V600E} for 24 h, stained with Annexin V-FITC and PI, and apoptosis was detected via flow cytometry. (**G**) Cell migration was assessed by wound healing assays. COLO320 and HCT116 cells were treated with PBS, EVs-NC or EVs-siBRAF^{V600E} for 24 h. The concentration of EVs-NC and EVs-siBRAF^{V600E} in all treatments was 50 μg/mL. The data are reported as the means ± SDs of the experiments ($n = 3$). Two-way ANOVA for (**A**) and (**B**), and one-way ANOVA for the others

EVs-siBRAF^{V600E} we constructed can inhibit the lung and liver metastases of BRAF^{V600E} colorectal cancer in vivo.

Inhibitory effects of therapeutic agents in BRAF^{V600E}-mutant CRC in PDX models

To further explore the efficiency of EVs-siBRAF^{V600E} in treating BRAF^{V600E}-mutant colorectal cancer, we utilized surgical resection of CRC tissues from a patient harboring the BRAF^{V600E} mutation to establish PDX models in BALB/c nude mice. When the PDX tumors reached approximately 100 mm^3 in size (approximately 10 days after implantation), the mice were divided into 3 groups and intravenously injected with PBS, EVs-NC, or EVs-siBRAF^{V600E} every 3 days for a total of 8 injections, as shown in Fig. 8A. We observed that tumor growth was significantly slower in the EVs-siBRAF^{V600E} treatment group than in the PBS and EVs-NC groups (Fig. 8B). The mice were sacrificed 3 days after the last treatment, and the tumors were extracted and weighed. The tumor volume and weight in the EVs-siBRAF^{V600E} group were significantly smaller than those in the EVs-NC and PBS groups (Fig. 8C, D). We sliced PDX tumor tissues and performed IHC assays, which revealed that all three groups exhibited pathological features characteristic of colorectal cancer. The expression levels of BRAF in the PDX tumor tissues of the EVs-siBRAF^{V600E} group were lower than those in the PBS and EVs-NC groups. Additionally, the phosphorylation levels of ERK1/2 were lower in the tumors treated with EVs-siBRAF^{V600E} than in those treated with PBS and EVs-NC (Fig. 8E).

To further validate the specificity of EVs-siBRAF^{V600E} for targeting the BRAF^{V600E} mutation in patient tissues, we obtained surgically resected CRC tissues from two patients with BRAF^{WT} (P1 and P2) and established PDX models (PDX1 and PDX2) accordingly. Similarly, in vivo experiments were conducted as show in Fig. 8A, with three groups of mice treated with PBS, EVs-NC, or EVs-siBRAF^{V600E}. We found that in PDX1 and PDX2 mice, the tumor growth rates were comparable between the EVs-siBRAF^{V600E} treatment group and the groups treated with PBS or EVs-NC (Fig. 8F, G). 3 days after the last treatment, the mice were euthanized, and the tumors were extracted. There were no significant differences in tumor volume or weight among the different treatment groups (Fig. 8H-K). These results further indicated that our therapeutic agent, EVs-siBRAF^{V600E}, can inhibit BRAF^{V600E}-mutant CRC while showing no significant therapeutic effects on BRAF^{WT} CRC derived from patient tissues. Thus, EVs-siBRAF^{V600E} exhibited specific therapeutic efficacy against BRAF^{V600E}-mutant colorectal cancer.

The targeting capability and systemic toxicity of therapeutic agents

Owing to the EPR effect, extracellular vesicles can passively accumulate in tumor tissues. Therefore, we speculated that our therapeutic agent would also accumulate in colorectal cancer tissues. We established a PDX model by implanting CRC tissue from the patients with the BRAF^{V600E} mutation into the left flank of nude mice. Extracellular vesicles labeled with DiD were injected intravenously into the tail vein of mice bearing PDX models. 24 h after injection, imaging revealed significant signals at tumor sites in both the EVs-NC and EVs-siBRAF^{V600E} groups (Fig. 9A, B). Thus, our constructed EVs-siBRAF^{V600E}, like EVs-NC, demonstrated the ability to target tumor sites.

To investigate the potential toxic side effects of our therapeutic agent, we collected important organs, including lung, liver, kidney, and spleen tissues, and blood from the aforementioned subcutaneous tumor models, as show in Fig. 7A. Important biochemical indicators of vital organs function in mouse serum were examined, and all parameters were within normal ranges for mice treated with PBS, EVs-NC, and EVs-siBRAF^{V600E} (Fig. 9C-H). Histological examination of the lung, kidney, spleen and liver tissues stained with hematoxylin and eosin (HE) revealed no significant changes in the structure or morphology of these four vital organs among the PBS, EVs-NC, and EVs-siBRAF^{V600E} groups (Fig. 9I-L). These results indicated that when used to treat colorectal cancer, our therapeutic agent cannot induce significant toxic side effects in vital organs.

Discussion

BRAF gene mutations have been detected in various types of tumors, including colorectal cancer. Among patients with colorectal cancer, approximately 7 ~ 15% carry a BRAF mutation [3, 29]. BRAF mutations are associated with the occurrence, progression, and drug resistance of tumors. These mutations lead to sustained activation of the downstream signaling molecules MEK1/2-ERK1/2,

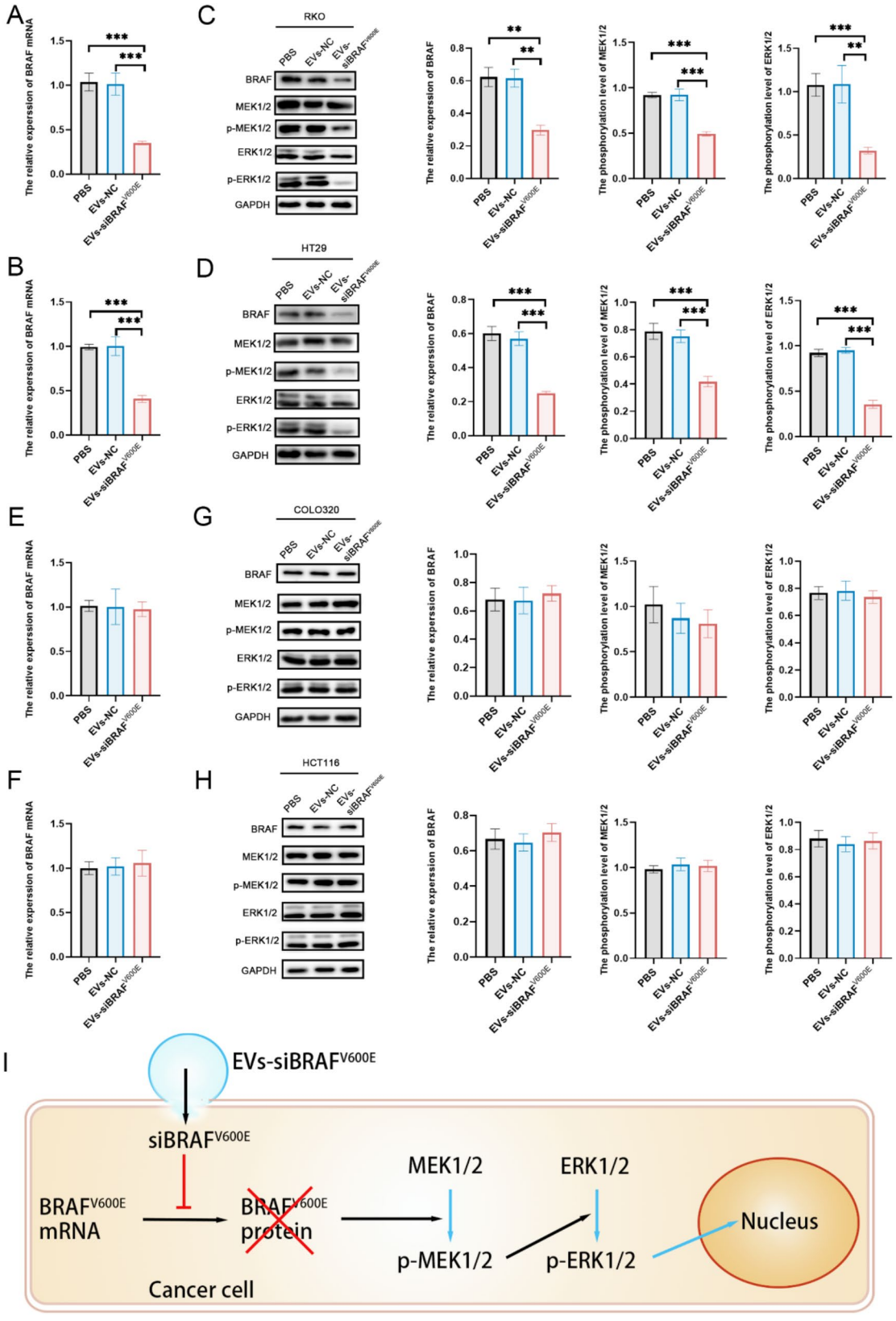

Fig. 6 (See legend on next page.)

(See figure on previous page.)

Fig. 6 EVs-siBRAF^{V600E} Inhibit BRAF-MEK1/2-ERK1/2 Signaling Pathway in BRAF^{V600E} CRC cells. (**A**) and (**B**) qRT-PCR analysis of BRAF transcription levels. RKO (**A**) and HT29 (**B**) cells were treated with PBS, EVs-NC or EVs-siBRAF^{V600E} for 24 h, followed by detection of BRAF mRNA levels. (**C**) and (**D**) WB analysis of BRAF expression levels and MEK1/2-ERK1/2 phosphorylation levels. RKO (**C**) and HT29 (**D**) cells were treated with PBS, EVs-NC or EVs-siBRAF^{V600E} for 24 h, and the BRAF protein levels and MEK1/2-ERK1/2 phosphorylation levels were measured. (**E**) and (**F**) qRT-PCR analysis of BRAF transcription levels. COLO320 (**E**) and HCT116 (**F**) cells were treated with PBS, EVs-NC or EVs-siBRAF^{V600E} for 24 h, followed by the detection of BRAF mRNA levels. (**G**) and (H) WB analysis of BRAF expression levels and MEK1/2-ERK1/2 phosphorylation levels. COLO320 (**G**) and HT29 (**H**) cells were treated with PBS, EVs-NC or EVs-siBRAF^{V600E} for 24 h, and the BRAF protein levels and MEK1/2-ERK1/2 phosphorylation levels were measured. The concentration of EVs-NC and EVs-siBRAF^{V600E} in all the treatments was 50 μg/mL. (**I**) Schematic illustration of the mechanism by which EVs-siBRAF^{V600E} treat CRC cells. The data are reported as the means ± SDs of the experiments ($n = 3$). One-way ANOVA followed by Tukey test multiple comparisons, *$p < 0.05$, **$p < 0.01$ and ***$p < 0.001$

promoting tumor growth [7]. Additionally, studies have shown that BRAF mutations may cause changes in tumor metabolism and hypoxia tolerance [30–32]. Therefore, in tumors with BRAF mutations, BRAF is a key therapeutic target. Currently, the most mature strategy for BRAF target therapy is BRAF inhibitors. several inhibitor drugs have already been approved for marketing [33]. Unfortunately, the efficacy of these inhibitors in BRAF-mutant CRC is not ideal [22, 23, 33]. Some studies involving multi-drug combination therapies, including BRAF inhibitors, have shown therapeutic effects in colorectal cancer, but these combination therapies significantly increase the cost of treatment for patients and expose them to a higher risk of multi-drug-related side effects [18]. Whether multi-drug combinations will increase the risk of resistance is also a concern that needs to be considered. The EVs-siBRAF^{V600E} we have developed have a different mechanism from inhibitors, as they directly downregulate the expression of the BRAF mutant protein. In our study, EVs carrying siRNAs targeting the BRAF^{V600E} mutation significantly inhibited the growth of BRAF-mutant CRC both in vitro and in vivo. Further validation of treatment effectiveness was conducted on CRC tissues from patients via the PDX model (Fig. 1). Furthermore, due to the different mechanisms, there may also be therapeutic effects in patients who are resistant to BRAF inhibitors and chemotherapy drugs, which is one of the directions for our future research. Gene therapy for tumors has also been reported, where other types of drug carriers, such as liposomes and nano-complexes, were used to deliver nucleic acid drug [34–37]. Our research is based on EVs as nucleic acid drug carriers.

Gene therapy has become a new strategy for disease treatment and tissue engineering research [38]. Small RNA gene therapy is a hotspot for the treatment of genomic diseases at the molecular level. Numerous studies have reported the effectiveness of small RNAs as therapeutic agents for various diseases [25, 39–41]. In this study, we designed siRNAs targeting BRAF mutations, which effectively reduced the level of mutant BRAF protein. However, small RNAs are unstable outside cells and prone to degradation, leading to loss of function, posing a challenge for their use as drugs. Therefore, small RNAs require suitable carriers to protect them from degradation. Liposomes and viruses are classical drug carriers. Some researchers used lentivirus-mediated RNA interference to inhibit the growth and metastasis of melanoma [35]. Other researchers attempted liposome-based delivery of small RNAs for treating melanoma [36]. However, the safety of viruses, liposomes and other polymers requires further research and discussion. EVs have an advantage in safety compared to viruses and liposomes. Unlike artificially synthesized liposomes and potentially pathogenic viruses, EVs are derived from cells, making them safer. Additionally, cationic polymers can disrupt the structure of negatively charged cell membranes, whereas EVs, derived from cell membranes, do not damage cell structures when delivering drugs. Therefore, EVs are virtually non-toxic. Viruses and liposomes are quickly cleared from the body, whereas EVs can evade clearance by monocytes and persist for a longer time [25, 42]. Since EVs derived from cells, they naturally carry some proteins on their surface. It has been found that the presence of surface proteins enhances the uptake of EVs by tumor cells [25]. The surface proteins of EVs, coupled with the EPR effect, make EVs more efficient in drug delivery in vivo [24, 25]. Other carriers require artificial modification to carry proteins or peptides to increase cell uptake and drug delivery efficacy. Therefore, EVs as drug carriers have the advantages of long retention time, high efficiency, and safety. Our in vivo experiments also revealed that EVs could be enriched in tumor areas without causing toxicity to vital organs.

The efficient loading of nucleic acid drugs into EVs is essential for their use as carriers. Some studies have reported the electroporation method [43], but subsequent research has indicated instability and instances of failed delivery via an electroporation-based approach [44]. Additionally, methods such as electroporation, ultrasonication, and saponification may disrupt the vesicle membrane structure. In our study, we employed a different strategy. We first stably expressed the siRNA construct in HEK293T cells and then collected EVs from the cell culture supernatant. Our experimental results demonstrated successful loading of siRNAs into EVs, which were then delivered to tumor cells, where they exerted their function.

Various types of cells can be used as EVs production platforms, with mesenchymal stem cells (MSCs) and HEK293T cells being the primary sources used to obtain

extracellular vesicles for drug loading. However, there is controversy regarding the impact of MSC-derived EVs on tumors. Some studies have reported that natural extracellular vesicles from MSCs can inhibit tumor growth in mouse models of ovarian cancer, liver cancer, multiple myeloma, and bladder tumors [45–47]. Conversely, other studies have shown that MSC-derived extracellular vesicles can promote angiogenesis and tumor growth in mouse xenograft models of gastric and colon cancers [48]. To avoid the uncertainties associated with the use of MSC-derived EVs in tumor therapy, we opted to use HEK293T cells to engineer cells to obtain EVs. Our experimental results also indicated that, EVs derived from HEK293T cells didn't significantly affect tumor cells compared with PBS.

However, challenges remain in the clinical application of EVs. There are currently no convenient and rapid methods for extracting a large number of high-purity EVs, limiting the use of EVs in clinical treatment. Existing methods for EVs extraction do not completely separate EVs from other impurities, which casts doubt on the clinical utility of EVs. Studies on the production and regulation of EVs may be needed to overcome these obstacles [49]. Due to the existence of major histocompatibility complexes (MHC) in the human body, there may be immune rejection reactions against allogeneic organs and cells [44]. HEK293T cells are allogeneic cells for patients, and the EVs produced by them may induce immune responses when injected into patients. Before EVs can be applied in clinical therapy, the potential issues arising from MHCs need to be addressed, and appropriate donor cells are crucial factors [44]. In addition, we have not yet designed appropriate surface proteins for extracellular vesicles in this study. This leads to accumulation of EVs in the other organs, which can reduce the drug delivery efficiency of EVs. Therefore, we will continue this line of research to increase the targeting of our therapeutic EVs.

PDX models are established from patient tumor specimens, which can maintain the same genetic background, histological characteristics and heterogeneity as the patient [50–53]. Some studies have shown that efficacy studies conducted on PDX models can more accurately reflect the drug response of patients, with a high degree of consistency between patients and PDX models [53–57]. Compared with CDX models, PDX models more closely resemble the actual patient's condition, especially in clinical scenarios where life expectancy and adverse effects limit the number of different drugs that can be tested on patients [58, 59]. In this study, we established PDX models from patients with CRC, and the results demonstrated that our therapeutic system showed good efficacy in $BRAF^{V600E}$ tumors but had no effect on BRAF wild-type tumors. These findings indicated that our therapeutic system offers precise treatment for CRC patients with the $BRAF^{V600E}$ mutation. However, PDX models also have some limitations. PDX models require the use of immunodeficient mice, which lack a functional immune system and thus cannot predict immune system changes or their impact on the study. Additionally, PDX models are personalized, and they also have drawbacks such as long construction times, low screening throughput, and high costs, which make it difficult to use PDX models on a large scale.

Conclusion

In this study, we constructed a cell-derived therapeutic system based on EVs and nucleic acid drugs against $BRAF^{V600E}$-mutant tumors. Through cellular experiments, we demonstrated that the therapeutic agent, EVs-si$BRAF^{V600E}$, specifically reduced the levels of BRAF in $BRAF^{V600E}$ CRC cells and suppressed the activation of MEK1/2 and ERK1/2, thereby inhibiting the growth and metastasis of $BRAF^{V600E}$ CRC cells. Additionally, we further explored the specific therapeutic efficacy of EVs-si$BRAF^{V600E}$ in $BRAF^{V600E}$ CRC via CRC cell line xenograft models and PDX models. Moreover, our therapeutic system is nontoxic and has targeting characteristics. The therapeutic system based on EVs and nucleic acid drugs carrying siRNAs targeting $BRAF^{V600E}$ that we designed provides a new approach for the treatment of mutant CRC, which has significance in basic research and clinical transformation. Our study also provides new clinical strategies and research directions for targeted therapy and personalized precision treatment of tumors with genetic mutations.

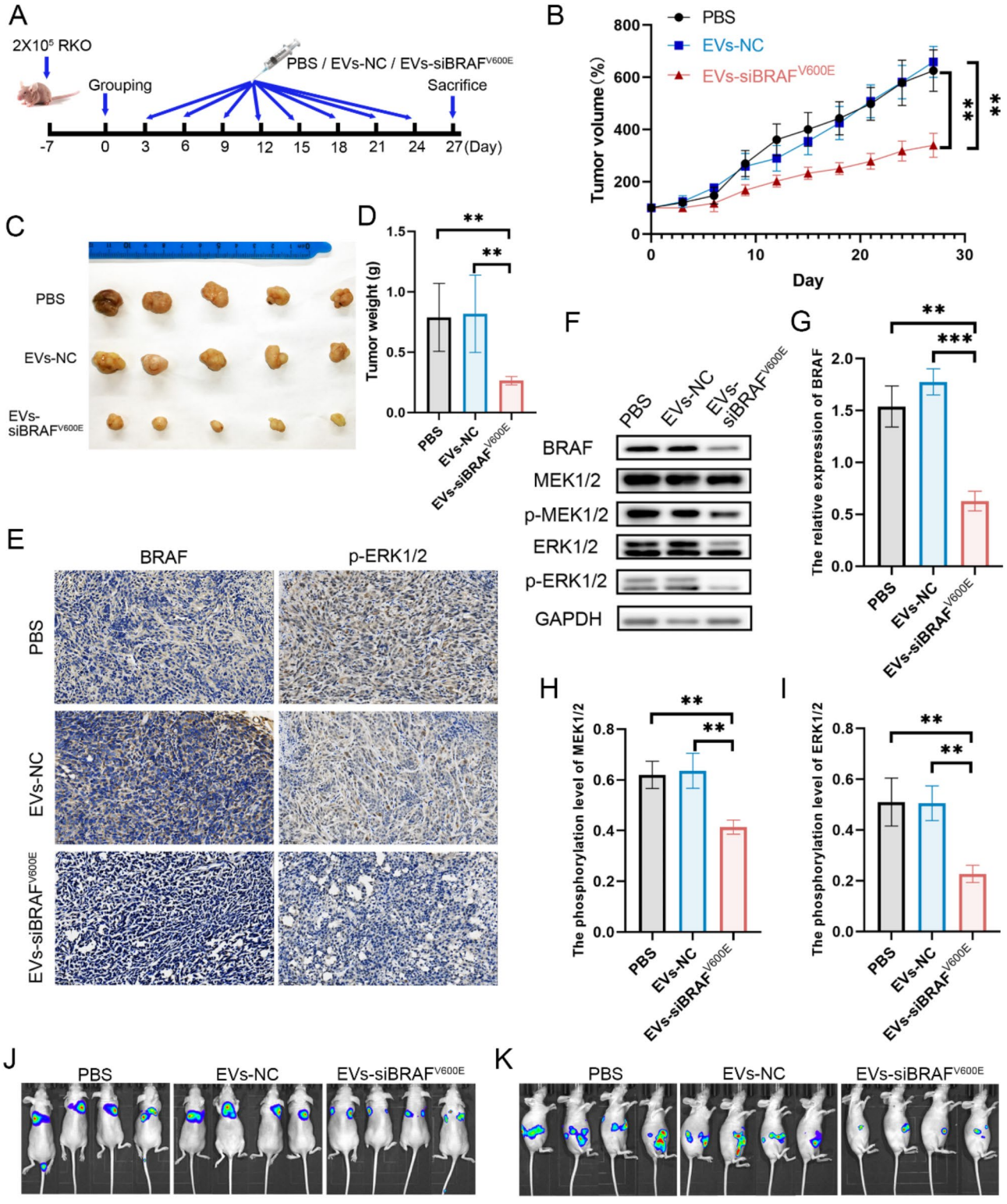

Fig. 7 EVs-siBRAF^{V600E} inhibit BRAF^{V600E} CRC in vivo. (**A**) Animal model handling protocol. (**B**) Subcutaneous tumor volume changes. Tumor volume measurements were performed every 3 days. (**C**) Images of the subcutaneous tumors in the three groups. (**D**) The weights of the subcutaneous tumors. (**E**) Immunohistochemistry images of BRAF and p-ERK1/2. Scale bar: 50 μm. (**F**)~(**I**) WB detection of BRAF expression and MEK1/2-ERK1/2 phosphorylation levels in subcutaneous tumor tissues. (**J**) Bioluminescence images of lung metastases. (**K**) Bioluminescence images of liver metastases. Each group of animals was treated with PBS, EVs-NC or EVs-siBRAF^{V600E}. Each mouse was injected with 20 μg of extracellular vesicles per injection. Subcutaneous tumors: $n = 5$ per group. Lung metastasis and liver metastasis: $n = 4$ per group. The data are reported as the means ± SDs of the experiments. Two-way ANOVA for (**B**), and one-way ANOVA followed by Tukey test multiple comparisons for the others, $^{*}p < 0.05$, $^{**}p < 0.01$ and $^{***}p < 0.001$

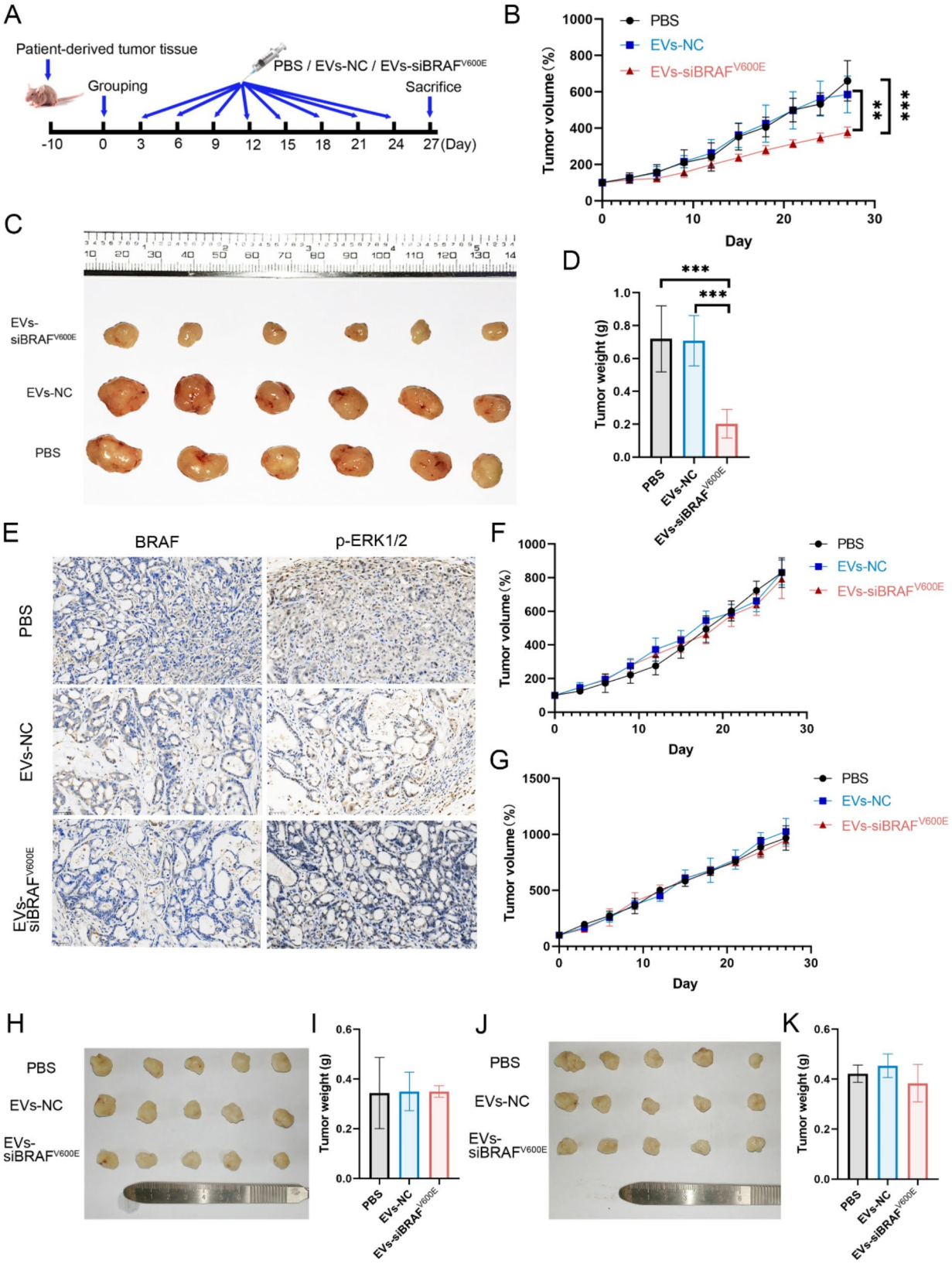

Fig. 8 (See legend on next page.)

(See figure on previous page.)

Fig. 8 Efficacy of EVs-siBRAF^{V600E} in human CRC PDX models. (**A**) PDX model handling protocol. (**B**) Subcutaneous tumor volume changes in the BRAF^{V600E} PDX models. Tumor volume measurements were performed every 3 days. (**C**)Images of subcutaneous tumors from the BRAF^{V600E} PDX models. (**D**) Subcutaneous tumor weights of the BRAF^{V600E} PDX models. (**E**) Immunohistochemistry images of BRAF and p-ERK1/2 in the BRAF^{V600E} PDX models. Scale bar: 50 μm. (**F**) and (**G**) Subcutaneous tumor volume changes in the BRAF^{WT} PDX models. Tumor volumes of BRAF^{WT} PDX1(**F**) and PDX2(**G**) were measured every 3 days. (**H**) Images of subcutaneous tumors from the BRAF^{WT} PDX1 models. (**I**) Subcutaneous tumor weights of the BRAF^{WT} PDX1 models. (**J**) Images of subcutaneous tumors from the BRAF^{WT} PDX2 models. (**K**) Subcutaneous tumor weights of the BRAF^{WT} PDX2 models. Each group of animals was treated with PBS, EVs-NC or EVs-siBRAF^{V600E}. Each mouse was injected with 20 μg of extracellular vesicles per injection. $N = 6$ for each group of BRAF^{V600E} PDX models. $N = 5$ for each group in the BRAF^{WT} PDX1 and PDX2 models. The data are reported as the means ± SDs of the experiments. Two-way ANOVA for (**B**), (**F**) and (**G**), and one-way ANOVA followed by Tukey test multiple comparisons for the others, $^{*}p < 0.05$, $^{**}p < 0.01$ and $^{***}p < 0.001$

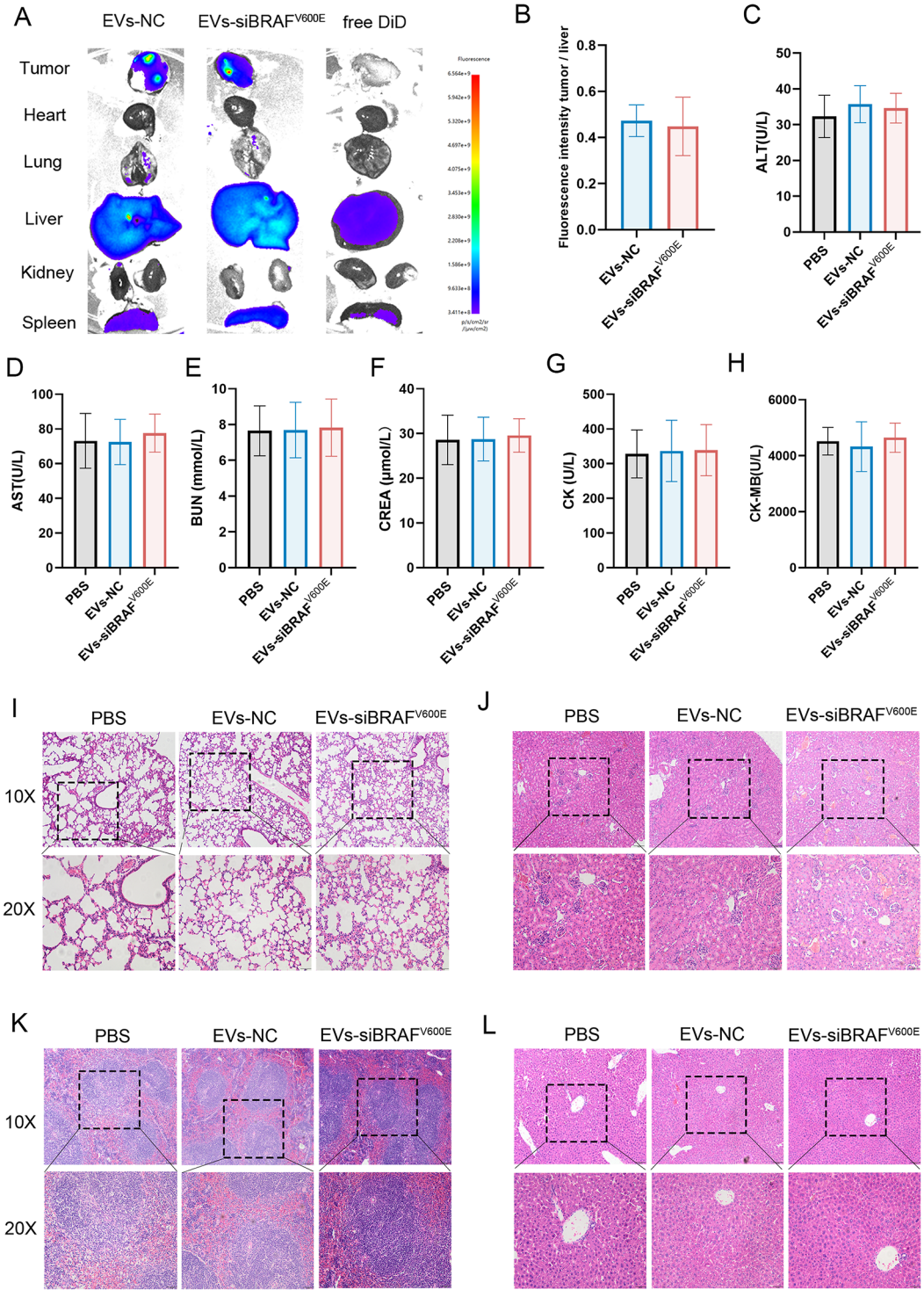

Fig. 9 Tumor targeting capability and safety of EVs-siBRAF^{V600E} in vivo. (**A**) Biodistribution images of EVs-NC or EVs-siBRAF^{V600E} in major organs and tumors. (**B**) Semi-quantitative analysis of the distribution in tumors. (**C**)~(**D**) After treatment with PBS, EVs-NC or EVs-siBRAF^{V600E}, related serum biochemistry indicators were analyzed, including hepatic function enzymes, such as ALT (**C**) and AST (**D**); renal function enzymes, such as BUN (**E**) and CREA (**F**); and cardiac function indicators, such as CK (**G**) and CK-MB (**H**), were analyzed in RKO xenograft models. (**I**) ~(**L**) Representative images of histological assessments of major organs. After treatment with PBS, EVs-NC and EVs-siBRAF^{V600E}, the lungs, kidneys, spleens and livers of RKO xenograft models from each group were collected. The data are reported as the means ± SDs of the experiments ($n = 5$). One-way ANOVA

Supplementary Information

The online version contains supplementary material available at https://doi.org/10.1186/s12951-025-03205-4.

Supplementary table 1. Primer sequence

Acknowledgements
Not applicable.

Author contributions
J.X., W.Z. and X.L. conceived and designed the study. L.Z., C.Y. and J.R. provided critical scientific input. D.W., L.W., W.Z., K.X., L.C., Z.G., K.X., D.H., Y.Z. and M.Y. performed the experiments. D.W., L.W., and W.Z. wrote the draft manuscript. D.W., L.W., W.Z. and J.X. revised the manuscript. All authors reviewed the manuscript.

Funding
This study was supported by grants from National Natural Science Foundation of China (No. 32371412, 32071349, 32471371, 82373163 and 82102598), Zhejiang Provincial Natural Science Foundation of China (No. LY24C100001, LY24E030002, LY23H160022 and LQ21H060008).

Data availability
No datasets were generated or analysed during the current study.

Declarations

Ethics approval and consent to participate
All the animal experiments were reviewed and approved by the Laboratory animal management and ethics committee of the Second Affiliated Hospital, Zhejiang University School of Medicine (approval number: 2024 – 170), and the use of human tumor tissues were approved by the Ethics Committee of Sir Run Run Shaw Hospital, Zhejiang University (Acceptance Number: 2024-2450-01).

Competing interests
The authors declare no competing interests.

Author details
[1]Department of Orthopedic Surgery, The Second Affiliated Hospital, School of Medicine, Zhejiang University, Hangzhou, Zhejiang 310009, PR China
[2]Orthopedics Research Institute of Zhejiang University, Hangzhou, Zhejiang 310009, PR China
[3]Key Laboratory of Motor System Disease Research and Precision Therapy of Zhejiang Province, Hangzhou, Zhejiang 310009, PR China
[4]Clinical Research Center of Motor System Disease of Zhejiang Province, Hangzhou, Zhejiang 310009, PR China
[5]Department of Colorectal Surgery, Sir Run Run Shaw Hospital, School of Medicine, Zhejiang University, Hangzhou, Zhejiang 310016, PR China
[6]Department of Orthopaedic Surgery, Sir Run Run Shaw Hospital, School of Medicine, Zhejiang University, Hangzhou, Zhejiang 310016, PR China

Received: 23 October 2024 / Accepted: 5 February 2025
Published online: 20 February 2025

References

1. Corcoran RB, Dias-Santagata D, Bergethon K, Iafrate AJ, Settleman J, Engelman JA. BRAF gene amplification can promote Acquired Resistance to MEK inhibitors in Cancer cells harboring the BRAF V600E mutation. Sci Signal. 2010;3(149):ra84.
2. Deng G, Bell I, Crawley S, Gum J, Terdiman JP, Allen BA, et al. BRAF mutation is frequently present in sporadic colorectal Cancer with methylated hMLH1, but not in Hereditary Nonpolyposis Colorectal Cancer. Clin Cancer Res. 2004;10(1):191–5.
3. Davies H, Bignell GR, Cox C, Stephens P, Edkins S, Clegg S, et al. Mutations of the BRAF gene in human cancer. Nature. 2002;417(6892):949–54.
4. De Roock W, Claes B, Bernasconi D, De Schutter J, Biesmans B, Fountzilas G, et al. Effects of KRAS, BRAF, NRAS, and PIK3CA mutations on the efficacy of cetuximab plus chemotherapy in chemotherapy-refractory metastatic colorectal cancer: a retrospective consortium analysis. Lancet Oncol. 2010;11(8):753–62.
5. Yaeger R, Chatila WK, Lipsyc MD, Hechtman JF, Cercek A, Sanchez-Vega F, et al. Clinical sequencing defines the genomic Landscape of Metastatic Colorectal Cancer. Cancer Cell. 2018;33(1):125–e1363.
6. Barras D, Missiaglia E, Wirapati P, Sieber OM, Jorissen RN, Love C, et al. BRAF V600E Mutant Colorectal Cancer subtypes based on Gene expression. Clin Cancer Res. 2017;23(1):104–15.
7. Peyssonnaux C, Eychène A. The Raf/MEK/ERK pathway: new concepts of activation. Biol Cell. 2001;93(1–2):53–62.
8. Grothey A, Fakih M, Tabernero J. Management of BRAF-mutant metastatic colorectal cancer: a review of treatment options and evidence-based guidelines. Ann Oncol. 2021;32(8):959–67.
9. Sinicrope FA, Shi Q, Smyrk TC, Thibodeau SN, Dienstmann R, Guinney J, et al. Molecular markers identify subtypes of stage III colon cancer associated with patient outcomes. Gastroenterology. 2015;148(1):88–99.
10. Jones JC, Renfro LA, Al-Shamsi HO, Schrock AB, Rankin A, Zhang BY, et al. Non-V600 BRAF mutations define a clinically distinct molecular subtype of metastatic colorectal Cancer. J Clin Oncol. 2017;35(23):2624–30.
11. Ullah R, Yin Q, Snell AH, Wan L. RAF-MEK-ERK pathway in cancer evolution and treatment. Sem Cancer Biol. 2022;85:123–54.
12. Fu L, Chen S, He G, Chen Y, Liu B. Targeting Extracellular Signal-regulated protein kinase 1/2 (ERK1/2) in Cancer: an update on pharmacological small-molecule inhibitors. J Med Chem. 2022;65(20):13561–73.
13. Yaeger R, Corcoran RB. Targeting alterations in the RAF–MEK pathway. Cancer Discov. 2019;9(3):329–41.
14. Jin H, Huang X, Pan Q, Ma N, Xie X, Wei Y, et al. The EIF3H-HAX1 axis increases RAF-MEK-ERK signaling activity to promote colorectal cancer progression. Nat Commun. 2024;15(1):2551.
15. Ma W, Chen Y, Xiong W, Li W, Xu Z, Wang Y, et al. STOML2 interacts with PHB through activating MAPK signaling pathway to promote colorectal Cancer proliferation. J Experimental Clin Cancer Res. 2021;40(1):359.
16. Ciombor KK, Strickler JH, Bekaii-Saab TS, Yaeger R. BRAF-Mutated Advanced Colorectal Cancer: a rapidly changing Therapeutic Landscape. J Clin Oncol. 2022;40(24):2706–15.
17. Prahallad A, Sun C, Huang S, Di Nicolantonio F, Salazar R, Zecchin D, et al. Unresponsiveness of colon cancer to BRAF(V600E) inhibition through feedback activation of EGFR. Nature. 2012;483(7387):100–3.
18. Nakayama I, Hirota T, Shinozaki E. BRAF Mutation in Colorectal cancers: from prognostic marker to Targetable Mutation. Cancers (Basel). 2020;12(11):3236.
19. Tournigand C, André T, Achille E, Lledo G, Flesh M, Mery-Mignard D, et al. FOLFIRI followed by FOLFOX6 or the reverse sequence in advanced colorectal cancer: a randomized GERCOR study. J Clin Oncol. 2004;22(2):229–37.
20. Fuchs CS, Marshall J, Mitchell E, Wierzbicki R, Ganju V, Jeffery M, et al. Randomized, controlled trial of irinotecan plus infusional, bolus, or oral fluoropyrimidines in first-line treatment of metastatic colorectal cancer: results from the BICC-C study. J Clin Oncol. 2007;25(30):4779–86.
21. Falcone A, Ricci S, Brunetti I, Pfanner E, Allegrini G, Barbara C, et al. Phase III trial of infusional fluorouracil, leucovorin, oxaliplatin, and irinotecan (FOLFOXIRI) compared with infusional fluorouracil, leucovorin, and irinotecan (FOLFIRI) as first-line treatment for metastatic colorectal cancer: the Gruppo Oncologico Nord Ovest. J Clin Oncol. 2007;25(13):1670–6.
22. Kopetz S, Desai J, Chan E, Hecht JR, O'Dwyer PJ, Maru D, et al. Phase II pilot study of Vemurafenib in patients with metastatic BRAF-Mutated colorectal Cancer. JCO. 2015;33(34):4032–8.
23. Gomez-Roca CA, Delord J, Robert C, Hidalgo M, von Moos R, Arance A, et al. 535P - encorafenib (Lgx818), an oral braf inhibitor, in patients (pts) with Braf V600E Metastatic Colorectal Cancer (Mcrc): results of dose expansion in an Open-Label, phase 1 study. Ann Oncol. 2014;25:iv182.
24. van der Meel R, Fens MHAM, Vader P, van Solinge WW, Eniola-Adefeso O, Schiffelers RM. Extracellular vesicles as drug delivery systems: lessons from the liposome field. J Control Release. 2014;195:72–85.
25. Kamerkar S, LeBleu VS, Sugimoto H, Yang S, Ruivo CF, Melo SA, et al. Exosomes facilitate therapeutic targeting of oncogenic KRAS in pancreatic cancer. Nature. 2017;546(7659):498–503.
26. Ai Y, Tian Y, Qiao J, Wang C, Li H. Yin-Yang philosophy for the design of anticancer drug delivery nanoparticles. Biomater Transl. 2024;5(2):144–56.
27. Cao Z, Liu J, Yang X. Deformable nanocarriers for enhanced drug delivery and cancer therapy. Exploration. n/a(n/a):20230037.

28. Avruch J, Zhang XF, Kyriakis JM. Raf meets Ras: completing the framework of a signal transduction pathway. Trends Biochem Sci. 1994;19(7):279–83.
29. Wang Y, Loree JM, Yu C, Tschautscher M, Briggler AM, Overman MJ, et al. Distinct impacts of KRAS, NRAS and BRAF mutations on survival of patients with metastatic colorectal cancer. JCO. 2018;36(15suppl):3513–3513.
30. Kumar SM, Yu H, Edwards R, Chen L, Kazianis S, Brafford P, et al. Mutant V600E BRAF increases Hypoxia Inducible Factor-1α expression in Melanoma. Cancer Res. 2007;67(7):3177–84.
31. Kang HB, Fan J, Lin R, Elf S, Ji Q, Zhao L, et al. Metabolic rewiring by oncogenic BRAF V600E links ketogenesis pathway to BRAF-MEK1 signaling. Mol Cell. 2015;59(3):345–58.
32. Xia S, Lin R, Jin L, Zhao L, Kang HB, Pan Y, et al. Prevention of Dietary-Fat-Fueled Ketogenesis attenuates BRAF V600E Tumor Growth. Cell Metabol. 2017;25(2):358–73.
33. Hertzman Johansson C, Egyhazi Brage S. BRAF inhibitors in cancer therapy. Pharmacol Ther. 2014;142(2):176–82.
34. Ruan W, Zhai Y, Yu K, Wu C, Xu Y. Coated microneedles mediated intradermal delivery of octaarginine/BRAF siRNA nanocomplexes for anti-melanoma treatment. Int J Pharm. 2018;553(1–2):298–309.
35. Sumimoto H, Miyagishi M, Miyoshi H, Yamagata S, Shimizu A, Taira K, et al. Inhibition of growth and invasive ability of melanoma by inactivation of mutated BRAF with lentivirus-mediated RNA interference. Oncogene. 2004;23(36):6031–9.
36. Tran MA, Gowda R, Sharma A, Park EJ, Adair J, Kester M, et al. Targeting V600EB-Raf and Akt3 using nanoliposomal-small interfering RNA inhibits cutaneous melanocytic Lesion Development. Cancer Res. 2008;68(18):7638–49.
37. Jadhav LA, Mandlik SK. Nanocarriers in skin cancer treatment: emerging drug delivery approaches and innovations. Nano TransMed. 2025;4:100068.
38. Esmaeili Y, Bidram E, Bigham A, Atari M, Nasr Azadani R, Tavakoli M, et al. Exploring the evolution of tissue engineering strategies over the past decade: from cell-based strategies to gene-activated matrix. Alexandria Eng J. 2023;81:137–69.
39. Tao SC, Yuan T, Zhang YL, Yin WJ, Guo SC, Zhang CQ. Exosomes derived from mir-140-5p-overexpressing human synovial mesenchymal stem cells enhance cartilage tissue regeneration and prevent osteoarthritis of the knee in a rat model. Theranostics. 2017;7(1):180–95.
40. Wang X, Zhang H, Bai M, Ning T, Ge S, Deng T, et al. Exosomes serve as nanoparticles to deliver anti-mir-214 to reverse chemoresistance to cisplatin in gastric Cancer. Mol Ther. 2018;26(3):774–83.
41. Lou G, Song X, Yang F, Wu S, Wang J, Chen Z, et al. Exosomes derived from mir-122-modified adipose tissue-derived MSCs increase chemosensitivity of hepatocellular carcinoma. J Hematol Oncol. 2015;8(1):122.
42. Ishida T, Kiwada H. Accelerated blood clearance (ABC) phenomenon upon repeated injection of PEGylated liposomes. Int J Pharm. 2008;354(1–2):56–62.
43. Alvarez-Erviti L, Seow Y, Yin H, Betts C, Lakhal S, Wood MJA. Delivery of siRNA to the mouse brain by systemic injection of targeted exosomes. Nat Biotechnol. 2011;29(4):341–5.
44. ichiro Ohno S, Takanashi M, Sudo K, Ueda S, Ishikawa A, Matsuyama N, et al. Systemically injected exosomes targeted to EGFR deliver antitumor microRNA to breast cancer cells. Mol Ther. 2013;21(1):185–91.
45. Roccaro AM, Sacco A, Maiso P, Azab AK, Tai YT, Reagan M, et al. BM mesenchymal stromal cell-derived exosomes facilitate multiple myeloma progression. J Clin Invest. 2013;123(4):1542–55.
46. Bruno S, Collino F, Deregibus MC, Grange C, Tetta C, Camussi G. Microvesicles derived from human bone marrow mesenchymal stem cells inhibit tumor growth. Stem Cells Dev. 2013;22(5):758–71.
47. Wu S, Ju GQ, Du T, Zhu YJ, Liu GH. Microvesicles derived from human umbilical cord Wharton's jelly mesenchymal stem cells attenuate bladder tumor cell growth in vitro and in vivo. PLoS ONE. 2013;8(4):e61366.
48. Liang X, Li C, Song J, Liu A, Wang C, Wang W, et al. HucMSC-Exo promote Mucosal Healing in Experimental Colitis by accelerating intestinal stem cells and epithelium regeneration via wnt signaling pathway. Int J Nanomed. 2023;18:2799–818.
49. Wang D, Zhang W, Zhang C, Wang L, Chen H, Xu J. Exosomal non-coding RNAs have a significant effect on tumor metastasis. Mol Ther Nucleic Acids. 2022;29:16–35.
50. Ding L, Ellis MJ, Li S, Larson DE, Chen K, Wallis JW, et al. Genome remodelling in a basal-like breast cancer metastasis and xenograft. Nature. 2010;464(7291):999–1005.
51. Li S, Shen D, Shao J, Crowder R, Liu W, Prat A, et al. Endocrine-therapy-resistant ESR1 variants revealed by genomic characterization of breast-cancer-derived xenografts. Cell Rep. 2013;4(6):1116–30.
52. DeRose YS, Wang G, Lin YC, Bernard PS, Buys SS, Ebbert MTW, et al. Tumor grafts derived from women with breast cancer authentically reflect tumor pathology, growth, metastasis and disease outcomes. Nat Med. 2011;17(11):1514–20.
53. Zhang X, Claerhout S, Prat A, Dobrolecki LE, Petrovic I, Lai Q, et al. A renewable tissue resource of phenotypically stable, biologically and ethnically diverse, patient-derived human breast cancer xenograft models. Cancer Res. 2013;73(15):4885–97.
54. Hidalgo M, Amant F, Biankin AV, Budinská E, Byrne AT, Caldas C, et al. Patient-derived xenograft models: an emerging platform for translational cancer research. Cancer Discov. 2014;4(9):998–1013.
55. Marangoni E, Vincent-Salomon A, Auger N, Degeorges A, Assayag F, de Cremoux P, et al. A new model of patient tumor-derived breast cancer xenografts for preclinical assays. Clin Cancer Res. 2007;13(13):3989–98.
56. Migliardi G, Sassi F, Torti D, Galimi F, Zanella ER, Buscarino M, et al. Inhibition of MEK and PI3K/mTOR suppresses tumor growth but does not cause tumor regression in patient-derived xenografts of RAS-mutant colorectal carcinomas. Clin Cancer Res. 2012;18(9):2515–25.
57. Keysar SB, Astling DP, Anderson RT, Vogler BW, Bowles DW, Morton JJ, et al. A patient tumor transplant model of squamous cell cancer identifies PI3K inhibitors as candidate therapeutics in defined molecular bins. Mol Oncol. 2013;7(4):776–90.
58. Garrido-Laguna I, Tan AC, Uson M, Angenendt M, Ma WW, Villaroel MC, et al. Integrated preclinical and clinical development of mTOR inhibitors in pancreatic cancer. Br J Cancer. 2010;103(5):649–55.
59. Ding N, Cui XX, Gao Z, Huang H, Wei X, Du Z, et al. A triple combination of atorvastatin, celecoxib and tipifarnib strongly inhibits pancreatic cancer cells and xenograft pancreatic tumors. Int J Oncol. 2014;44(6):2139–45.

Publisher's note